공학석사학위논문

유성 기어박스의 진동기반 고장 진단을 위한 저가형 센서의 정량적 성능 평가

Quantitative performance evaluation of a knock sensor for vibration-based fault diagnosis in a planetary gearbox

2017 년 8 월

서울대학교 대학원

기계항공공학부

김 건

유성 기어박스의 진동기반 고장 진단을 위한 저가형 센서의 정량적 성능 평가

Quantitative performance evaluation of a knock sensor for vibration-based fault diagnosis in a planetary gearbox

지도교수 윤 병 동

이 논문을 공학석사 학위논문으로 제출함

2017 년 6 월

서울대학교 대학원

기계항공공학부

김 건

김 건의 공학석사 학위논문을 인준함

2017 년 5 월

위 원 장 조 맹 효 (인)

부위원장 윤 병 동 (인)

위 원 김 도 년 (인)

Abstract

Quantitative performance evaluation of a knock sensor for vibration-based fault diagnosis in a planetary gearbox

Keon Kim
School of Mechanical and Aerospace Engineering
The Graduate School
Seoul National University

A gearbox is a critical component in rotating machinery. Timely prediction of gearbox faults is of great importance to minimize unscheduled machine downtime. Most existing gearbox diagnosis studies to date have focused on the development of gearbox diagnosis algorithms using costly vibration sensors. However, traditional vibration sensors are cost-prohibitive in some applications; thus, pushing to the use of low-cost accelerometers, such as knock sensors. Knock sensors are known to be inexpensive and good for application (i.e., in diesel engines) to detect high-frequency vibrations. This study examines a planetary gearbox with a knock sensor and evaluates the ability of the knock sensor.

This study develops a novel quantitative sensor evaluation process for fault diagnosis. The performance of the sensor is evaluated in terms of vibration measurement performance and fault diagnosis performance. Vibration measurement performance is evaluated by assessing the sensor's noise level through an experiment using an electro-dynamic transducer. Fault diagnosis performance is evaluated by analyzing the vibration signal obtained from a faulty gear through gearbox feature engineering to determine whether the fault has been separated or not.

Two ideas are proposed in this study. First, quantitative metrics are used to evaluate the performance of the sensor. The vibration measurement performance of the knock sensor is evaluated using the signal-to-noise ratio (SNR). The stable frequency range of the knock sensor for fault diagnosis is defined based on the SNR value. For fault diagnosis evaluation, fault separation capability is carried out by probability of separation (PoS) and Fisher discriminant ratio (FDR). Second, a new application of the base-signal (i.e., difference signal used in Time Synchronous Averaging) is proposed to be used for fault diagnosis. The filtered signal obtained by an alternative signal processing method (i.e., autoregressive-minimum entropy deconvolution (AR-MED) or spectral kurtosis (SK)) is used as a difference signal when there is no tachometer. The frequency range and periodicity of the fault signal are analyzed to determine the availability of the feature calculated with the newly applied differential signal.

Two case studies are presented to demonstrate the effectiveness of the proposed sensor evaluation process and metric: 1) a one-stage planetary gearbox in a wind-turbine rig tester and 2) a swing reduction gear (two-stage planetary gearbox) in an excavator. Through the research in this study, it is concluded that a knock sensor can be used for fault diagnosis of a gearbox.

Keywords: Excavator fault diagnosis
Knock sensor
Planetary gearbox
Sensor evaluation

Student Number: 2015-22705

Table of Contents

List of Tables

List of Figures

Nomenclature

N	The total number of data points in the time record
d	Difference signal
$\bar{d}$	Mean value of the difference signal
P_{NS}	Probability of failure
$f_{ci}(s)$	Probability density function (PDF) of the i^{th} class
$F_{ci}(s)$	Cumulative distribution function (CDF) of the i^{th} class
$\breve{x}_{ci}$	Median value of the i^{th} class
μ_i	Mean value of the i^{th} distribution
σ_i	Standard deviation of the i^{th} distribution
A	Root mean square values of the signal amplitude
F_c	Central frequency of the frequency range with the highest kurtosis
Bw	Bandwidth of the frequency range with the highest kurtosis
F_f	Periodic frequency of the fault as determined by envelope analysis

Chapter 1. Introduction

1.1 Background and Motivation

Various studies have been conducted on how to detect the presence of an abnormality by measuring the vibration of a mechanical device. In recent years, improvements in computing power have led to the development of various fault diagnosis and prognostics methods to predict the remaining useful life of a device or engineered system. Traditionally, these studies, which require significant development and maintenance costs, have concentrated on large-device industries, such as power plants or mining equipment, aerospace industries, and automobiles. In the construction machinery industry, some technologies for prognostics have been developed and applied for large mining equipment. Arakawa (2002) introduced a condition monitoring system for mining equipment based on operational data [1]. He, He, and Zhu (2008) suggested a fault detection method for an excavator's hydraulic system based on dynamic principal component analysis [2].

Recently, many construction equipment manufacturers have tried to apply fault diagnosis or prognostics technologies for small or low-cost construction equipment. However, the cost of vibration sensors prevents their use in some applications, thus pushing companies toward the use of low-cost accelerometers. Therefore, in this research, we evaluated the feasibility of using low-cost accelerometers with a vibration-based fault diagnosis algorithm for condition monitoring of a planetary gearbox. The planetary gearbox constitutes the swing reduction gear of the excavator. This research employs a knock sensor, a sensor that is frequently used to

detect high-frequency impulse vibration signals generated from irregular combustion in diesel engines. Because the knock sensor had never been used for detection of a planetary gear failure, it was first necessary to evaluate the basic performance of the sensor. Based on initial performance evaluation, available frequency ranges for fault diagnosis were suggested. Following this step, we defined a signal processing method to enhance performance of the knock sensor for fault diagnosis of the gearbox.

1.2 Scope of Research

In the research outlined in this thesis, two ideas are proposed, in the following research areas: 1) an evaluation methodology is proposed to define sensor performance using quantitative metrics, and 2) a new application of the base-signal of a feature is developed, which is used for the fault diagnosis.

In the research thrust 1, quantitative metrics are used to evaluate the performance of the sensor. The vibration performance of the knock sensor is evaluated using the signal-to-noise ratio (SNR). The stable frequency range of the knock sensor for fault diagnosis is defined based on the SNR value. For fault diagnosis evaluation, fault separation capability is carried out by probability of separation (PoS) and Fisher discriminant ratio (FDR) techniques.

Research thrust 2 proposes a new application of the base-signal of a feature for fault diagnosis. When there is no tachometer, the filtered signal obtained by the alternative signal processing method (i.e., autoregressive-minimum entropy deconvolution (AR-MED) and spectral kurtosis (SK)) is used as a difference signal. The frequency range is then analyzed and the periodicity of the fault signal is

examined to determine the availability of the feature, as calculated by the newly applied differential signal.

1.3 Structure of the Thesis

Chapter 2 provides a brief review of the technical background and methodology for fault diagnosis in a planetary gearbox, and gives an overview of the selection of sensors. Chapter 3 introduces performance evaluation of the knock sensor, using Signal-to-Noise Ratio (SNR) for vibration measurement. Chapter 4 shows the proposed method for evaluation of the knock sensor in terms of fault diagnosis, based on the evaluation results outlined in Chapter 3. In this process, three signal processing methods are used, and a new method of applying the difference signal is introduced. Chapter 5 summarizes the research and presents the conclusions of the thesis.

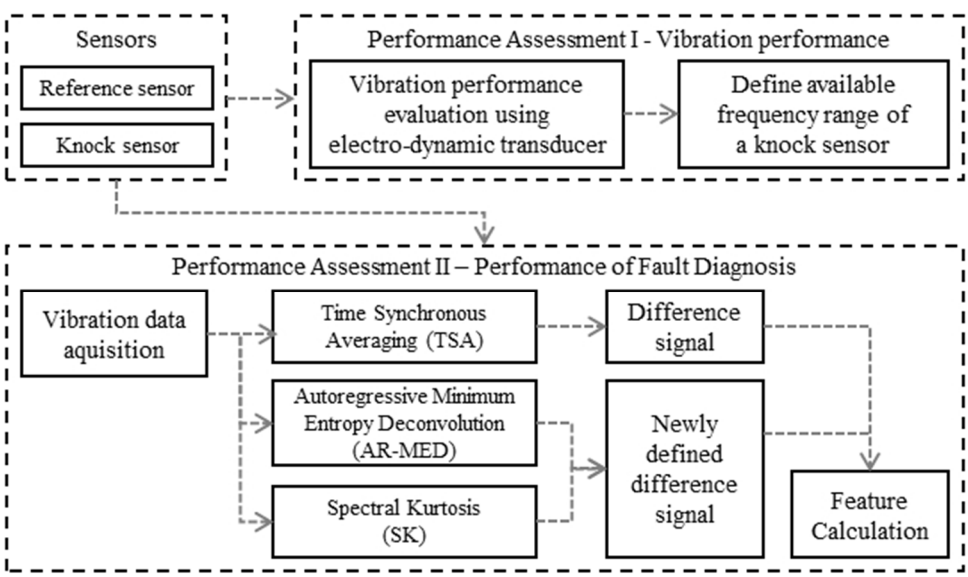

Figure 1-1 Framework for sensor evaluation

Chapter 2. Technical Background

2.1 Fault Diagnosis in a Planetary Gearbox

In conventional planetary gearbox fault diagnosis, gear feature engineering can be divided into two procedures: signal processing and feature (i.e., health data) calculation. In general, signal processing can be performed either in the time domain or in the frequency domain. To calculate the health data to be used in this study, the difference signal (i.e., the signal that remains when the gear mesh frequency, harmonics, and sideband components are removed from the raw signal) must be obtained through signal processing [3]. After that, health data, such as FM4, M6A, and M8A, which are known to show good performance in detecting gear surface damage, are calculated based on the difference signal [4],[5].

2.1.1 Vibration Characteristics of a Faulty Gearbox

The first step of performing fault diagnosis for a gearbox is to determine what kind of faults occur in the target system. For example, if the shaft is misaligned, if the surface of a target part is worn, or if there is a crack that could cause the part to break. Fault identification is necessary because the type of vibration generated by each fault is different. For example, surface defects of gear teeth are reported to cause resonance, while generating shock waves that have resonance frequencies. Li, Ding, He and Lin (2016) classified failures that can occur in gears into three types: 1) steady-type faults, 2) impact-type faults, and 3) compound-type faults. In steady-type faults, such as tooth geometrical error, mild wear, and mild misalignment, the

sidebands around the GMF can be emphasized. Impact-type faults (i.e., fractures, cracks, and ruptured teeth) have been shown to cause abnormal frequencies in the high-frequency range, such as system resonant frequencies and harmonics [6].

For the research described in this paper, a second-stage sun gear inside the swing reduction gear of an excavator was selected as the target part for fault diagnosis. Figure 2 shows the results of Failure Modes, Effects, and Criticality Analysis (FMECA) performed on swing devices in the last 5 years as part of this work. 64% of the total failures were confirmed to be due to a gear fault. Of the gear faults, 93% were found to be an impact-type fault, and 64% occurred in the sun gear.

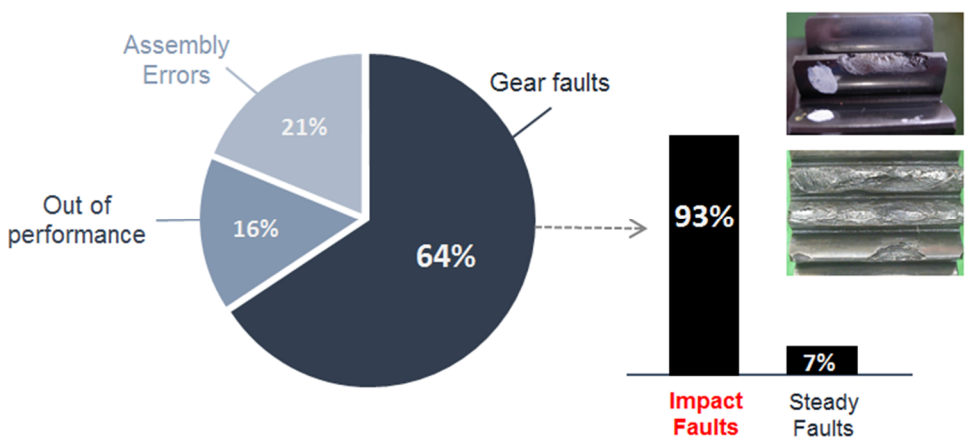

Figure 2-1 Results of FMECA for the swing reduction gear, as observed since 2009

2.1.2 Signal Processing Methods

Fault diagnosis requires a technique that identifies the state of the machine from its vibrations, as vibrations can be a signal of the condition of the gearbox. The vibrations that occur in gearboxes are very complex in structure, but provide a lot of information. In order to understand the information conveyed by the vibrations, unnecessary signals must be reduced through signal processing methods. Signal processing methods can be classified into three types according to their methodology. Specific types include: 1) time-domain analysis; 2) frequency-domain analysis; and 3) time-frequency analysis. In this study, fault diagnosis is performed using 1) Time Synchronous Averaging (TSA) and Autoregressive-Minimum Entropy Deconvolution (AR-MED) of time-domain analysis and 2) Spectral Kurtosis (SK) of frequency-domain analysis [7], [8], [9].

1) Time Synchronous Averaging (TSA)

TSA is a method that can determine a single cycle according to the rotational frequency of the target gear. The entire signal can then be cut according to the cycle and the signal can be averaged to reduce the noise signals. A schematic of TSA is shown in Figure 2-2. It is necessary to convert unequally-sampled time series data into equally-sampled time series data using a resampling process in the first step. At this time, the tach-signal obtained from an encoder is essential. For example, for heavily worn gears, the time synchronous averaged signal is used as-is. To monitor the evolution of the damage from the earliest stage, the gear mesh frequency (GMF) and harmonic components are removed from the averaged signal; the result is called the *residual signal*. Removing the sideband components from this

residual signal results in what is called the *difference signal*. This signal can be used to detect a fault of the gear surface.

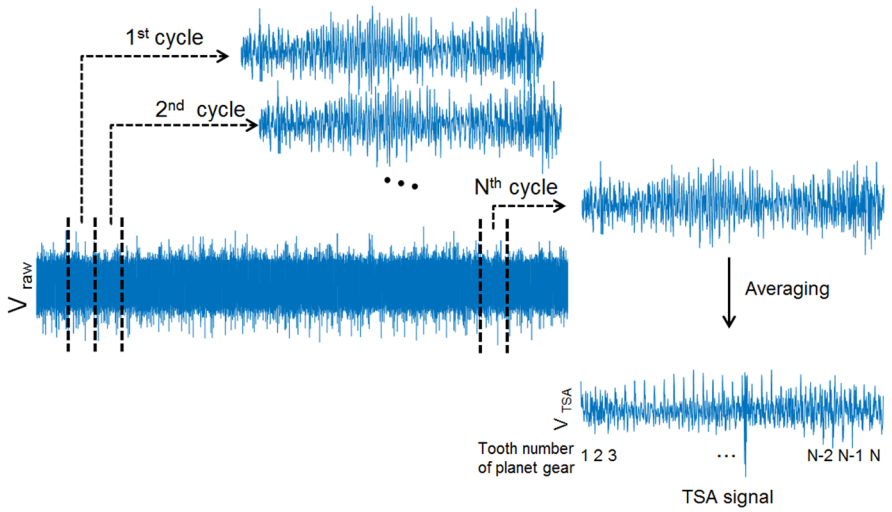

Figure 2-2 Schematic of Time Synchronous Averaging

2) Autoregressive-Minimum Entropy Deconvolution (AR-MED)

Endo et al. (2007) proposed an enhanced method of detecting a gear fault through combination of two filters, as shown in Figure 2-3, specifically: 1) an Autoregressive (AR) filter was used to extract a deterministic signal; and 2) a Minimum Entropy Deconvolution (MED) filter was employed that emphasizes the impact signal.

The AR filter estimates a deterministic signal using a certain amount of data and builds an AR model based on the estimated signal. Removing the estimated signal from the raw signal leaves the non-deterministic signals (i.e., noises, fault-related signals, and components that are due to uncertainties). The MED filter can emphasize the impact signal due to a

fault by using the high-order statistical (HOS) characteristics of the signal, especially the phase information that is provided by the kurtosis [9].

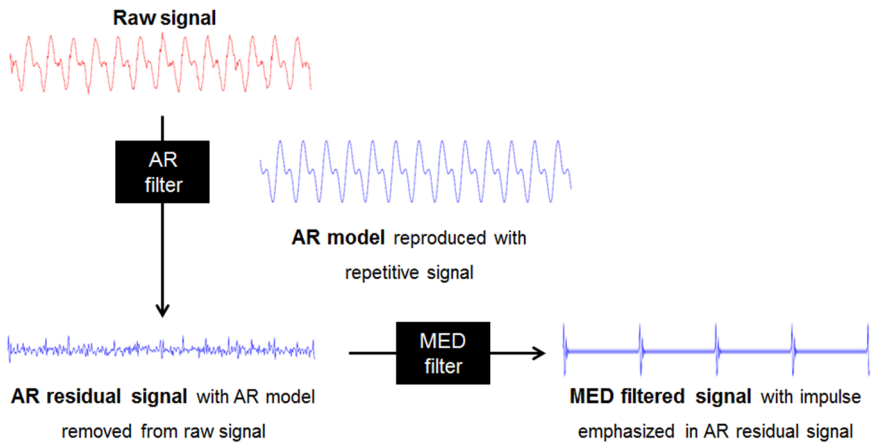

Figure 2-3 Schematic of AR-MED

3) Spectral Kurtosis (SK)

The Spectral Kurtosis (SK) technique was developed by Antoni and Randall (2006) as the enhanced frequency domain signal processing method. This method is capable of selecting the most critical frequency range for fault diagnosis of the system. In this method, the kurtosis is calculated by dividing the entire frequency range step by step, and the center frequency and the bandwidth of the highest kurtosis region are found. Thereafter, in order to check whether a fault has occurred, frequency analysis of the envelope signal of the region is performed to check the intervals of the peaks due to a fault. The SK technique is shown in Figure 2-4.

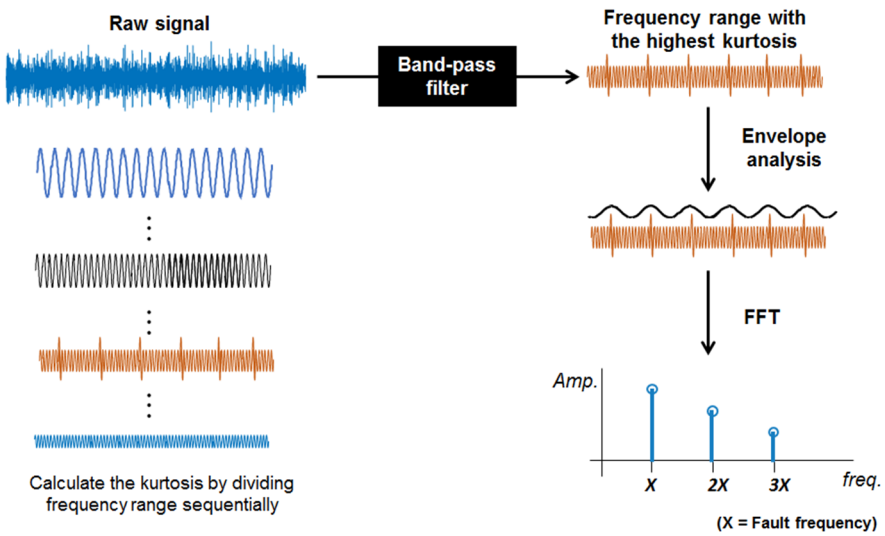

Figure 2-4 Process flow of Spectral Kurtosis

2.1.3 Features for Fault Diagnosis

1) M8A

More than a dozen different features have been introduced that can be used for diagnostics and prognostics of gearboxes through various signal processing techniques [10]. In this research, M8A, which is known to be specialized in detecting a failure due to gear surface damage [5], will be used. The M8A is calculated as described below.

$$\text{M8A} = \frac{N^3 \sum_{i=1}^{N} (d_i - \bar{d})^8}{\left[\sum_{i=1}^{N} (d_i - \bar{d})^2\right]^4} \tag{2.1}$$

where d is the difference signal and, $\bar{d}$ is the mean value of the difference signal, and N is the total number of data points in the time record.

The difference signal is defined as a signal that removes the GMF, its harmonics, and the sidebands from the signal of one cycle that is averaged based on the rotation information obtained through the TSA. This signal can represent the fault frequency more prominently because noises and vibrations related to the rotation of the gear are eliminated. Additional information about the difference signal will be given in Chapter 4.

2) Probability of Separation (PoS)

Probability of Separation is a class-separation metric that has been proposed to confirm the relative separation capability between distributions in a partially separated state [11]. PoS is based on the idea of load-strength interference. It is defined as follows, from calculation of the probability of failure when a load exceeding the strength is applied.

$$P_{NS} = \int_{-\infty}^{\infty} f_{c1}(x) F_{c2}(x) dx \quad for \ \tilde{x}_{c1} \leq \tilde{x}_{c2} \tag{2.2}$$

where $f_{c1}(s)$ and $F_{c2}(s)$ represent the probability density function (PDF) of class 1 and the cumulative distribution function (CDF) of class 2, respectively, while $\tilde{x}_{c1}$ and $\tilde{x}_{c2}$ correspond to the median values of classes 1 and 2. Here, PoS is calculated as:

$$\mathrm{PoS} = (\mathrm{e}^{(1-2\times \mathrm{P_{NS}})} - 1)/(\mathrm{e} - 1) \tag{2.3}$$

PoS gives a result of "0" if the distribution of feature values overlaps perfectly; it gives a result of "1" if the distribution is not overlapped at all.

3) Fisher Discriminant Ratio (FDR)

The FDR is defined as Eq. (2.4), using the mean and variance that can easily be obtained from the two distributions [12]. The numerator indicates the difference between the two-class means, while the denominator normalizes the variances of the two classes. The larger the separation of the two distributions, the larger the FDR. However, when used for non-normal distributions, it can show incorrect information.

$$FDR = \frac{\left(\mu_i - \mu_j\right)^2}{\sigma_i^2 + \sigma_j^2} \tag{2.4}$$

where μ_i and σ_i represent the mean and standard deviation of the i^{th} distribution.

2.2 Overview of Sensor Selection

The purpose of this chapter is to describe how a suitable sensor can be selected for fault diagnosis in a specific application (i.e., the rotating part of a piece of construction equipment). Because there is little research on fault diagnosis for rotating parts of construction equipment, consideration of various constraints of general fault diagnosis is essential. In particular, the selection of sensors is very important. The number of essential sensors for large wind turbine generators has been specified in prior work, as maintenance and fault diagnostics are frequently used for rotating parts in wind turbines [13]. The cost of sensors is not a major consideration, as it can be less than 1% of the total price of the equipment, even if many high-performance accelerometers are attached for stable condition monitoring in the case of wind turbines. On the other hand, even if only one sensor

of the same type and cost as used in the wind turbine is implemented, the cost of the construction machine is over 20% greater than the price of the parts to be diagnosed. Therefore, it is important to select a sensor that minimizes the cost, while securing a certain level of performance as compared to traditional sensors.

2.2.1 Specification of Accelerometer

Accelerometers are usually supplied with user manuals, specification sheets, and calibration certificate sheets. Various indexes are indicated on the specification sheet; these are important factors in selecting the accelerometer. When selecting an accelerometer, performance factors such as sensitivity, resolution, frequency range, accuracy, and impact limit – as well as the condition of the sensor environment and cost – have a great influence. [14]. Factors that have a particularly important impact on sensor selection include the sensitivity, resolution, and frequency range; these can be used to determine the *measurability* (i.e., how well-suited the sensor is to the particular application).

Sensitivity refers to the rate at which a sensor converts vibration input to electrical output. This value is directly proportional to the amplitude of the acceleration that the accelerometer can measure. The desired sensitivity depends on the level of the signal being measured. When measuring the magnitude of small vibrations or their fluctuating flow, a clean signal (i.e., high SNR) should be obtained with a sensor of high sensitivity. Conversely, to measure shock events with high amplitudes, sensors with low sensitivity may have enough accuracy.

Resolution is typically specified in bits that can be used to calculate the resolution in units of acceleration. For example, if the accelerometer has a resolution of 16 bits, it means that it has 2^{16} (65,536) acceleration levels or

measurable bins. When the measurement range is ± 1 g, it means a resolution of 0.00003 g (200/65536), which is the minimum measurable acceleration level. In relation to the sensitivity described above, the higher the resolution, the finer the analysis of the fluctuation of small vibrations.

The *frequency range* specification shows the maximum deviation of the sensitivity to the frequency range of the vibration that the sensor can measure. The tolerance bandwidth of the frequency range can be specified in percent and / or dB, where the standard bands are ± 5%, ± 10%, ± 1dB, and even ± 3dB. However, for accurate measurement results, it is recommended to keep the ± 5% standard that is used for calibration. This is because the accelerometer maintains the highest performance (i.e., the fluctuation of the measured value can be small).

Cost must sometimes be considered as a factor in order to secure desired measurability. As noted in the introduction of Chapter 2, especially in the area of condition monitoring and fault diagnosis, the cost of loss due to failure of the target system is often very large. However, cost can also be a very important specification for condition monitoring, especially when a large number of sensors must be installed or when the price of the sensor(s) that must be placed in the target system is significant. The threshold of the sensor cost may vary depending on the profit margin of each product, but the lower, the better.

In addition, several conditions of a sensor's operating environment are also important to consider. These conditions include the sensor’s usable temperature, resistance to external impact, size, weight, fixing method, and resistance to oil and dust.

2.2.2 Selection of a Knock Sensor

This section covers the selection of both traditional sensors and low-cost sensors for fault diagnosis. Table 2-1 shows the results of selecting three reference sensors and three low-cost sensors. The candidates for the sensors are selected based on frequency range, sensitivity, and measurement range.

Table 2-1 Brief specifications of sensor candidates

Sensor configuration	Manufacturer & Product no.	Frequency Range	Sensitivity	Measurement Range
Reference I	PCB Piezotronics - 621B40	1.6 to 30000Hz (±3dB)	10mV/g	±500g
Reference II	PCB Piezotronics - 601A02	0.17 to 10000Hz (±3dB)	500mV/g	±10g
Reference III	PCB Piezotronics - 605B01	0.5 to 5000Hz (±3dB)	100mV/g	±50g
Low-cost I	Analog Devices Inc. - ADXL132	125 to 1600Hz	43LSB/g	±12g
Low-cost II	STMicroelectronics - LIS2DE12TR	0.5 to 2690Hz	5 to 64 LSB/g	±2g to ±16g
Low-cost III	Continental Automotive - Customized for usage	3000 to 18000Hz	17 to 30 mV/g	Customized

Reference sensors are selected from several traditional sensors manufactured by the same manufacturer according to the specifications outlined for the target system, as described earlier. Low-cost sensors are chosen to be able to achieve maximum performance under a certain cost. Of the options, the sensors to be used in the research described in this paper were selected according to the frequency characteristics calculated as described in Section 2.1.1. Specifications were defined through preliminary experiments of the fault diagnosis system for the system of interest (i.e., the planetary gearbox of the swing reduction gear in an excavator). Detailed specifications of the final selected traditional sensor and low-cost sensor are shown in Table 2-2.

A knock sensor, selected here as the low-cost sensor, is widely used to detect shock events in vibration signals in the thousands of hertz range due to the irregular combustion in diesel engines. These sensors are classified into resonance and non-resonance types. The resonance type is good at detecting failure because the shock frequency due to knocking and the resonance frequency of the piezoelectric material in the sensor are similar. The non-resonance type, referred to as a flat-response type, is relatively low in detection but is useful for identifying shock events in various frequency ranges. The non-resonance type knock sensor adopted in this study was applied to the engine of an excavator equipped with the diagnostic target planetary gearbox. Even if the sensitivity of the fault signal is lower than that of the reference sensor, the detecting range of the fault frequency can still be better, because the frequency range is wide. In terms of cost effectiveness, a knock sensor is about a tenth of the cost of a traditional sensor.

Table 2-2 Comparison of specifications between the reference and the knock sensor

Classification	Reference accelerometer	Knock sensor
Manufacturer	PCB Piezotronics	Continental Automotive
Model No.	601A02	Customized for use
Price	About $500	Under $50
Purpose	General use	Shock events
Type	Piezoelectric	Piezoelectric (Flat-response)
Pros and cons	Inner circuit High stability High accuracy	Simple structure Need to ground Wide sensitivity range
Frequency Range	0.47 to 4000Hz (±5%) 0.33 to 5000Hz (±10%) 0.17 to 10000Hz (±3dB)	3 to 18kHz
Sensitivity	51mV/(m/s^2) (±20%)	1.7 to 3.7 mV/(m/s^2) at 5kHz Output@5kHz+15% at 8kHz Output@5kHz+30% at 13kHz Output@13kHz+100% at 18kHz

Chapter 3. Knock Sensor Evaluation from the Viewpoint of Vibration Measurement

3.1 Conventional Sensor Assessment Method

The conventional method of evaluating accelerometers is based on ISO 16063, which specifies the method of calibrating the accelerometer. Both an absolute method and a comparison method are available for calibration. First, the absolute method involves testing the sensor by subjecting it to a known, accurate, and reliable standard of nature. The sensor is checked to determine whether in the static state it shows the value of the gravitational acceleration in the forward direction and shows a negative value in the inverted state. It is also checked to see if it shows a value within an error of about 0.25% in the free-fall state. This method is mainly suitable for the inspection process that typically occurs immediately after the sensor's manufacturing. Second, the comparison method utilizes a reference sensor that has been calibrated by a certified laboratory. The same excitation is applied to the reference sensor and the target sensor, and the results are compared. These methods can be useful when developing new sensors or when using existing sensors for new purposes. For the purposes of this research, the comparison method seems more appropriate to confirm the performance of the sensor for vibration measurement. In some studies, the performance of a MEMS accelerometer is compared to a common accelerometer to ensure reliability in performance [15],[16]. To verify the performance of the newly developed knock sensors, E.Pipitone and L.D'Acquisto compared the features of their vibration performance to those of commercial sensors [17].

As described above, the absolute method can confirm the zero calibration in the static state of the sensor; however, the absolute method has the disadvantage that performance for vibration measurement cannot be verified. The comparison method can compensate for the shortcomings of the absolute method. The comparison method, though, has the disadvantage of being unable to make quantitative comparisons. In the above studies, it is confirmed whether the phase and magnitude are similar to each other. If there is an error, a correction method is suggested, or a performance comparison is made between a signal obtained by mounting a new sensor and a reference sensor to a specific system. These approaches, however, fall short of being able to quantitatively show whether the new sensor is available for purpose. In order to compensate for this, the following sections describe the performance of sensors in terms of quantified value via Signal-To-Noise ratio (SNR).

3.2 Signal-to-Noise Ratio (SNR)

Signal-to-Noise Ratio (SNR) is a measure that compares the level of an ideal signal to the level of background noise [18]. SNR is used mainly for the purpose of checking the quality of a signal to be analyzed after signal processing a raw signal [19]. Another purpose is to verify the specifications of an accelerometer, or to verify that the sensor background noise meets the criteria during periodic calibrations [20]. SNR can also be used as a quantitative metric to verify the effects of changes during the development or improvement of signal processing methods [21].

SNR is simply defined as the ratio of signal power to noise power, as shown below.

$$SNR = 10\log_{10}\left[\left(\frac{A_{signal_{voltage}}}{A_{noise_{voltage}}}\right)^2\right] \quad (2.1)$$

where A is the root mean square value of the signal amplitude.

No standards regarding the limit of the SNR exist, because SNR mainly depends on system and the filtering sequence. In image processing, a modest SNR* value is known to be 20dB [22], [23],[24].

3.3 Method of Estimating the SNR

This section describes how to estimate and calculate the SNR. In order to use SNR as a quantitative performance metric that expresses the vibration measurement performance of a sensor, its value must be calculated. As described earlier, SNR is the ratio of the desired signal to the unwanted signals (i.e., noises). The mathematical model of vibration can completely separate the two signals; however, when calculating the SNR from a measured signal it is almost impossible. A process flow of the methodology used to estimate the SNR can be seen in Figure 3-1. The shaker is excited with arbitrary sinusoidal wave conditions to receive time-domain signals from the sensor. These signals are transformed into a frequency-domain signal through Fast-Fourier-Transform (FFT). Then a notch filter is used to extract the desired signal and that signal is subtracted from the raw signal to obtain the noisy signal. SNR can be estimated by substituting the two obtained signals into Equation 2.1. The frequency range for this experiment was selected to be from 10Hz to 6kHz by considering the following four points: 1) GMF and its harmonics

are in the range of several tens to several hundred hertz, 2) the frequency range of the knock sensor, as guaranteed by the manufacturer, is 3 to 18kHz, 3) the frequency range with a 10% error level in the reference accelerometer is 0.33 to 5000Khz, and 4) the maximum excitation frequency of the electro-dynamic transducer (i.e., a shaker) used in the performance evaluation is 6.5KHz.

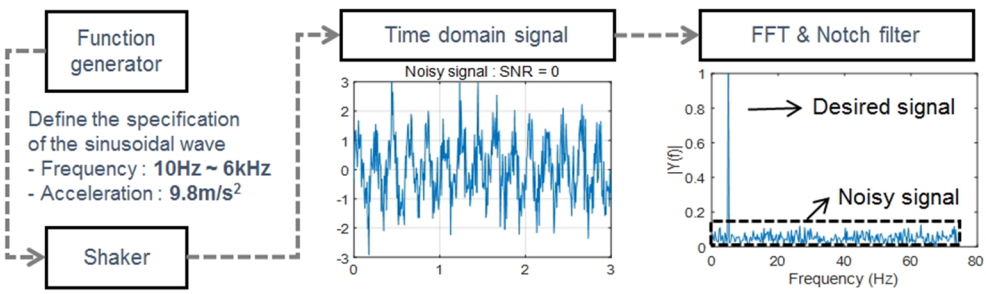

Figure 3-1 Process flow for the SNR estimation method

3.4 Results and Discussion

Figure 3-2 shows the results of using six samples per sensor type. The SNR of the reference sensor is over 45dB in the entire frequency range of the experiment. Since SNR is a system-dependent metric, there is no standard for limiting values; however, the appropriate SNR for signal processing is about 20 dB (i.e., the desired signal power is 10 times the noise power), so the reference accelerometer can be used as the reference for vibration measurement of the knock sensor.

Although the deviation between samples from the knock sensor is larger than those from the reference sensor, the knock sensor has a level equal to or higher than that of the reference sensor from the frequency range above about 2 kHz. The

average SNR value for the reference sensor is from 2kHz to 6.5kHz is 63.2dB and for the knock sensor is 68.0dB, which is about 10% higher. Manufacturers of knock sensors do not guarantee sensor performance below 3kHz, but the results of this experiment show that this sensor can be used from 2kHz. Although the SNR value is more than 20dB in the frequency range below 2kHz, the reliability would be low because the SNR fluctuates as the frequency range changes.

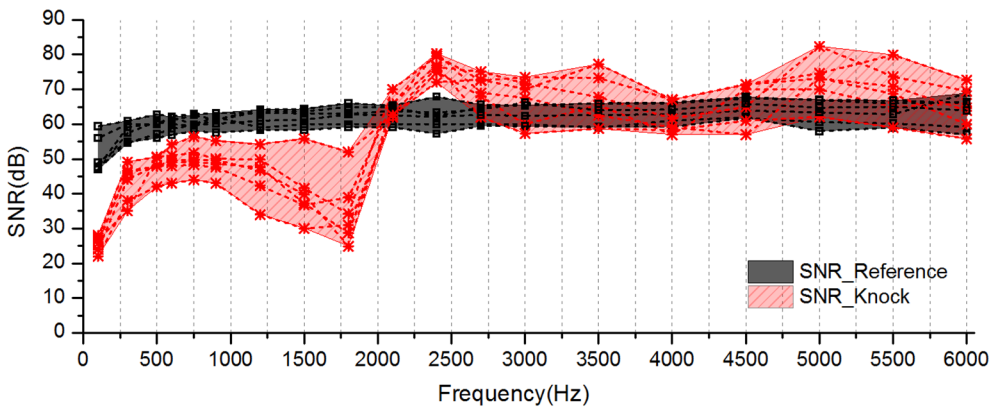

Figure 3-2 SNR of the reference sensor (black with square) and the knock sensor (red with star) by frequency range

Chapter 4. Knock Sensor Evaluation from the Viewpoint of Fault Diagnosis

Through the research outlined in Chapter 3, it has been confirmed that the knock sensor exhibits a vibration measurement performance similar to that of a reference sensor in the frequency range above 2 kHz. Based on these results, this chapter aims to quantitatively evaluate the performance of the knock sensor for fault diagnosis. First, Section 4.1 provides an introduction to the methods of fault diagnosis for planetary gearboxes. Then, a discussion is provided about how to use quantitative metrics for fault diagnosis using knock sensors [25].

4.1 Review of Fault Diagnosis

4.1.1 Model-based Methods

There have been many studies examining ways to predict the static and dynamic characteristics of a system by constructing a model. There are typically many assumptions and simplifications needed to build a model. While these assumptions make it difficult to verify a model's accuracy, models are still useful due to the time and cost savings provided over experimentation in real systems. Even in the case of planetary gears, models are very useful. Prior researchers have proposed methods for modeling the surface damage of gear teeth and analyzing the effect of the damage on the gear mesh stiffness [26]. Other work has compared gear dynamics of normal and faulty gears. [27] Another study suggests a methodology to detect faults based on the data and statistically estimate the damage level of gear teeth

[28]. There are also studies that simulate the response of vibrations to infer vibration characteristics through a model [29], [30].

4.1.2 Signal Processing Based Methods

Many of the studies on state monitoring and fault diagnosis of planetary gearboxes utilize signal processing methods. Signal processing methods can be classified into three types, as described in Section 2.1. Time domain and frequency domain methods, which are of primary interest in the research described in this paper, are briefly reviewed here.

1) Time-domain Analysis

   Time-averaged and statistical indicators are used to represent time domain analysis. If the rotation information can be obtained from a tachometer, it is relatively easy and straightforward to perform fault diagnosis with time-domain analysis, as compared with other methodologies. TSA can be used to calculate the average time for tooth-to-tooth vibration of the planet gear and the sun gear [31],[32], or various statistical measures can be used to assess the health of the planetary gearbox [33],[34]. However, some statistical indicators cannot accurately detect the fault on the system level test. Since the vibration characteristics due to the fault is influenced by various sources occurring at the operation conditions and at the system level [35].

2) Frequency-domain Analysis

The above-mentioned time-domain method (i.e., TSA) minimizes noise through averaging, and takes advantage of the fact that signals that arise due to failure are relatively prominent in that condition. Due to the frequency characteristics of various signals that arise from the complex structure of the planetary gearbox, there is a possibility that fault diagnosis cannot be done. The basic algorithm for frequency analysis is Fourier Transform (FT) or Fast Fourier Transform (FFT) [36]. Initially, Fourier transform was used directly for fault diagnosis, but now it is used as a basic process for frequency analysis. Typical methods of frequency analysis are 1) MED filter, which can enhance the fault detection performance by emphasizing the fault signals, and 2) SK, which analyzes the frequency sequentially to find the part with the highest kurtosis.

4.1.3 Discussion

The process of the fault diagnosis using the above-mentioned signal processing methods can be briefly described as follows: 1) graph the frequency characteristics using the model 2) determine statistical features using TSA and 3) find the kurtosis value using frequency domain analysis. Although the statistical features are quantitative and can represent fault types, the excavator, which is the target system of this paper, does not have an encoder. An encoder is a prerequisite of TSA. The kurtosis is also quantitative, but the accuracy of the fault characteristics identified can be relatively low compared to the statistical features.

4.2 Fault Diagnosis using Two Types of Difference Signals

The technical hurdles for fault diagnosis of a planetary gearbox in an excavator using a low-cost sensor can be summarized as follows.

1) A cost-effective sensor that shows stable vibration measurement performance at frequency range over 2kHz needs to be applied.
2) The target system has an encoderless condition and thus cannot use TSA-based features with fault characteristics.
3) Features capable of quantitative comparison of the reference sensor and the proposed knock sensor need to be selected.

To overcome these three hurdles, the following methodology is applied. In order to solve the first hurdle, faulty specimens in which the frequency that arises due to fault is prominent in the high frequency range, impact-type fault specimens, are selected. To overcome the second hurdle, we obtain the TSA-based feature through the frequency domain signal processing method. In this process, signal processing methods that can take advantage of characteristics of a knock sensor will be used. Finally, a quantitative performance comparison is performed with the class separation metrics that were calculated from the fault diagnosis features.

4.2.1 Definition of Difference Signal

From among the TSA-based signals mentioned in Chapter 2, here, we utilize the difference signal to calculate the features that are specific to sensing gear surface damage. This difference signal is obtained by removing the gear mesh frequency

(GMF), harmonics, and sideband components from the time synchronous average signal. The frequency-domain characteristics of the TSA-based signals are graphically shown in Figure 4-1. In Figure 4-1 (a), the frequency characteristic is shown, in which the noise is remarkably reduced. In Figure 4-1 (b), sideband components are emphasized by removing GMF. This is advantageous for detecting frequency characteristics that arise due to heavy wear. In Figure 4-1 (c), the sideband components are removed from the residual signal of Figure 4-1 (b), to show the influence of the frequency that is due to the characteristics of the system, rather than the rotation.

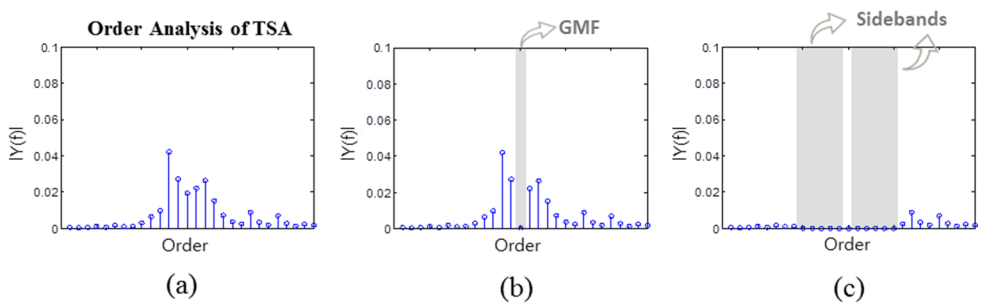

Figure 4-1 Frequency-domain characteristics of the TSA-based signals
(a): Time synchronous averaged signal, (b): Residual signal, (c): Difference signal

4.2.2 Methodology for Estimation of the Difference Signal

As described above, the difference signal can highlight the influence of the frequency of an impact-type fault that affects the vibration characteristics of the system. The difference signal highlights these characteristics by removing the frequency information associated with the rotation. Even if other signal processing methods are used, the results can be used as a difference signal if the results have

the effect of emphasizing a frequency that is caused by a fault. Schematic diagrams using time-domain signals are shown in Figure 4-2. The TSA signal in Figure 4-1 (a) shows a definite fault impact on the signal of one revolution of the gear. In Figure 4-1 (b) and (c), unlike in TSA, the signals of the whole range are targeted; however, the impacts that are due to a fault are noticeable, compared to the raw signal. Whether prominent fault impacts in the time domain show physical identity in the frequency domain will be discussed in the next chapter through experimental results.

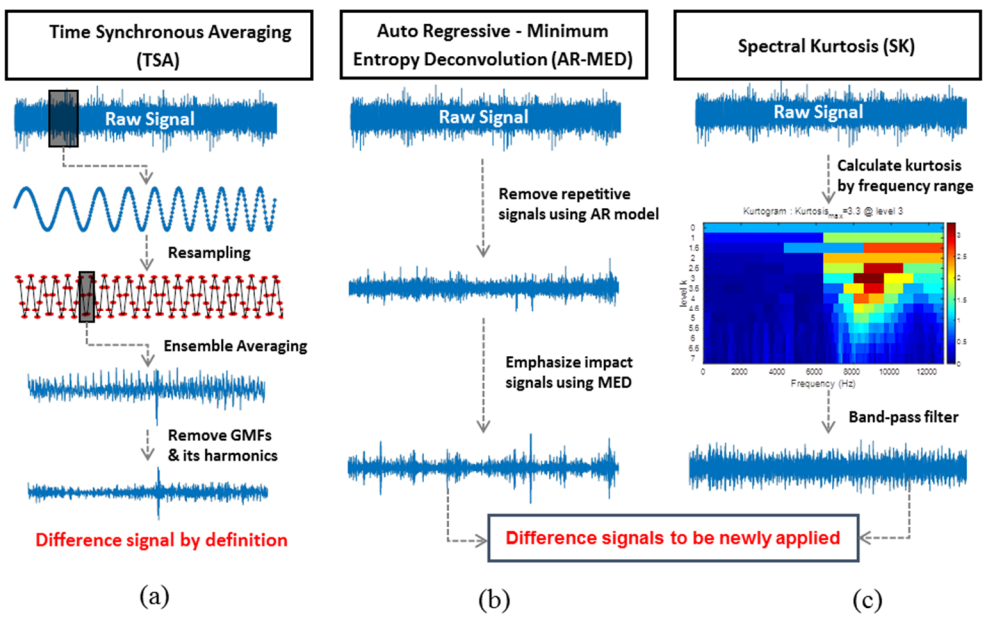

Figure 4-2 Schematic diagram of time-domain signals from different signal processing methods:

(a): Time synchronous averaging,

(b): Auto Regressive – Minimum Entropy Deconvolotion, (c): Spectral Kurtosis

4.3 Results and Discussion

4.3.1 Description of Experiments

a) Target Gearboxes

Because this research is the first time vibration-based fault diagnosis has been used for excavators' planetary gearboxes, a RIG tester was used first and an actual vehicle experiment was conducted. The RIG tester, which simulates a 2.5 MW wind turbine, is composed of two single-stage planetary gearboxes, one of which is equipped with a faulty gear specimen in the gearbox close to the high-speed shaft. The appearance and specifications of the WT RIG tester and gearbox are shown in Figure 4-3 and Table 4-1, respectively.

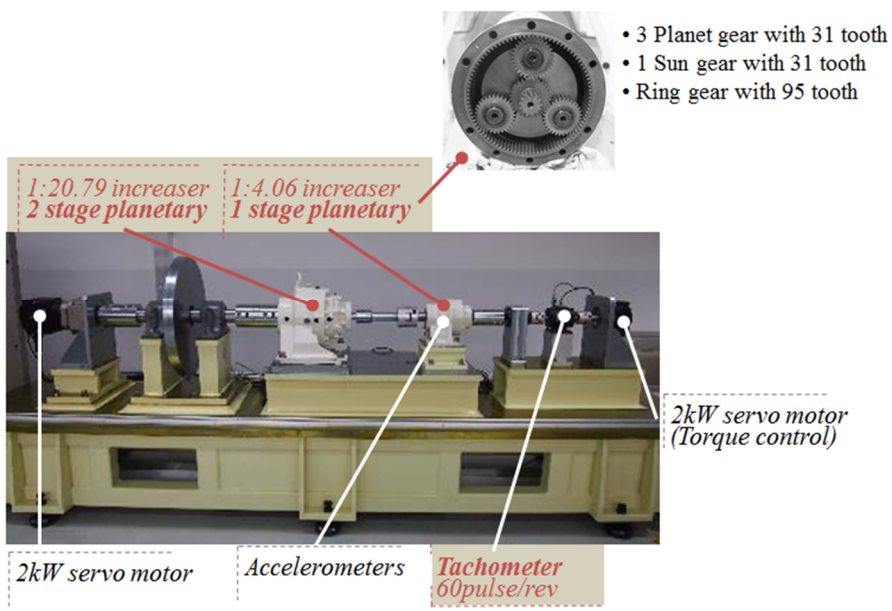

Figure 4-3 Wind turbine RIG tester

Table 4-1 Specifications of the WT RIG tester

Components	Qty.	Specifications
Input motor	1	2kW servo motor (Torque input)
Control motor	1	2kW servo motor (Torque control)
2 stage planetary gearbox	1	1:20.79 increaser
1 stage planetary gearbox	1	1:4.06 increaser
Accelerometers	8	500mV/g (Range:±10g)
RPM sensor(Tachometer)	1	60pulse/rev

The appearance and specifications of the target excavator and the planetary gearbox of interest are shown in Figure 4-4 and Table 4-2.

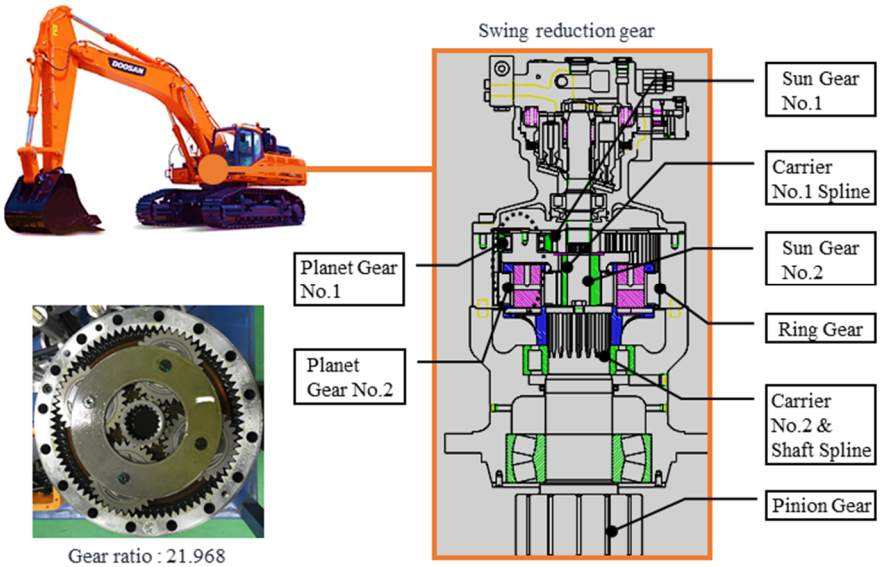

Figure 4-4 Target excavator and planetary gearbox

Table 4-2 Specifications of the planetary gearbox in the excavator used in this study

Stage	Gear ratio	Gear	Qty.	# of gear teeth
1st	5.053	Sun	1	19
		Planetary	4	28
2nd	4.348	Sun	1	23
		Planetary	4	26
Total	21.968	Ring	1	77

b) Design of Faulty Specimens

As introduced in Chapter 2, the characteristics of the fault frequency are projected differently in the vibration signal depending on the type of gear fault. As described in Chapter 3, for a knock sensor, reliable vibration measurement performance is displayed in areas over the 2 kHz range. Depending on the rotational speed of the gear system, the GMF can show the fault signal prominently in that area; however, usually the first GMF with the largest vibration magnitude is in the lower frequency range. The impact-type faults to be used in the experiments of the two cases in this study are shown in Table 4-3. Case 1 (i.e., WT RIG tester) is tested in a well-controlled environment, so specimens are used ranging from a small line crack to an extreme condition (i.e., absence of one gear tooth). Since Case 2 (i.e., the excavator case) is the vehicle level test with various variables, the fault specimens used are increasing in level, starting from the smallest crack.

Table 4-3 Dimension of gear tooth faults in the planetary gearbox test

Classification	ID	Shape	Description of the gear and fault
Case 1 (Rig test)	Crack I	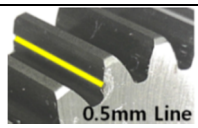	**0.5mm** along the tooth profile across the tooth face (100% line) on the pitch line in a **planetary gear**
	Crack II	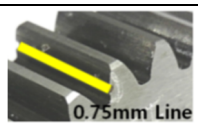	**0.75mm** along the tooth profile across the tooth face (100% line) on the pitch line in a **sun gear**
	One tooth removed		One tooth machined along the root circle line in a **planetary gear**
Case 2 (Vehicle)	Crack III	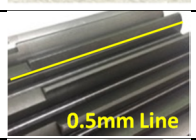	**0.5mm** along the tooth profile across the tooth face (100% line) on the pitch line in a **2nd stage sun gear**
	Crack IV	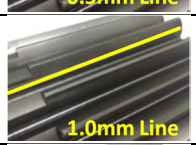	**1.0mm** along the tooth profile across the tooth face (100% line) on the pitch line in a **2nd stage sun gear**
	Crack V	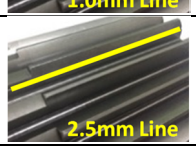	**2.5mm** along the tooth profile across the tooth face (100% line) on the pitch line in a **2nd stage sun gear**

c) Design of Experiments

Experiments were performed using three failed specimens for two different specs. Signals that arise due to the vibration of gears are modulated in phase and amplitude by rotational speed and torque [37],[38]. Since these effects cannot be compensated under encoderless conditions, the rated speed and rated torque of each system are applied. The rig tester can be used to acquire data for a long time; however, the vehicle application reduces the acquisition time to about one minute. Even under these conditions, one Hunting Tooth Cycle (HTC) is used as a dataset criterion to obtain a minimum of 10 data sets from one specimen for statistical analysis. The HTC refers to the cycle in which a particular gear tooth meshes with its counter gear [39]. For example, when a fault is applied to a planetary gear in the WT RIG tester, it means that the tooth (one of 31 teeth) is again in contact with the first tooth of first ring gear (one of 95 teeth). Using the HTC reduces the influence of variables such as the meshing conditions between each tooth.

Table 4-4 Design of experiments

Case	Speed of input shaft [RPS]	Torque of target shaft [Nm]	Data acquisition time [sec]	Hunting tooth cycles [sec]	# of datasets for feature calculation [set]
1	25.0	4	60	≈5	10
2	21.7	≈600	60	≈6	10

4.3.2 Comparison of Fault Diagnosis using Signal Processing Results

Prior to comparing the performance of the quantitative sensors in terms of fault diagnosis, it is necessary to qualitatively confirm the trends of the fault signals and the differences among the sensors by comparing to the three signal analysis methods used. Under an encoderless condition, when applying a methodology that utilizes TSA-based difference signals, it is necessary to check if the signal processing method is causing physical errors.

First, the signals are identified according to the signal analysis method for three failure specimens of the WT RIG tester. Results are obtained from the vehicle experiment by performing analysis in the same manner. At this time, 10 sets of data (approximately 60 seconds) are used to acquire the tendency of the vibration data. If the data length is too short, the minimum data length is determined by referring to the length of HTC mentioned above because there may be large filtering errors or variations after filtering, depending on the defect size. Each signal processing method is checked to determine whether the frequency range due to the same fault is similar, and comparison between the two sensors is performed.

a) TSA

In the time domain, the peak due to the fault of the raw signal and the difference signal is confirmed through TSA. In the frequency domain, the FFT residual signal (a signal obtained by extracting a FFT signal of normal state from a FFT signal with a fault) is used to compare the frequency range due to the fault in the two sensors. Only the WT RIG tester that is capable of signal acquisition from an encoder (i.e., tachometer) can have results using TSA.

Figure 4-5 shows the TSA results of the reference sensor according to the size

of the fault in the WT RIG tester. The peak due to the failure is clearly confirmed not only in the TSA signal in (a) but also in the difference signal in (b). Since TSA checks the signal based on one rotation of the gear after reducing the noise, the position information of the faulty gear can be checked. In the last graphs (FFT Residual), many frequency sources are found in entire frequency range. The area in the dotted line represents the estimate of the part of the frequency that is due to a fault in each fault case. The accuracy of this part will be compared later with the results of other signal processing methods. In the knock sensor results shown in Figure 4-6, it is possible to detect faults, however, it is confirmed that there is a lot of noise in the signals compared to the noise observed in the signal from the reference sensor.

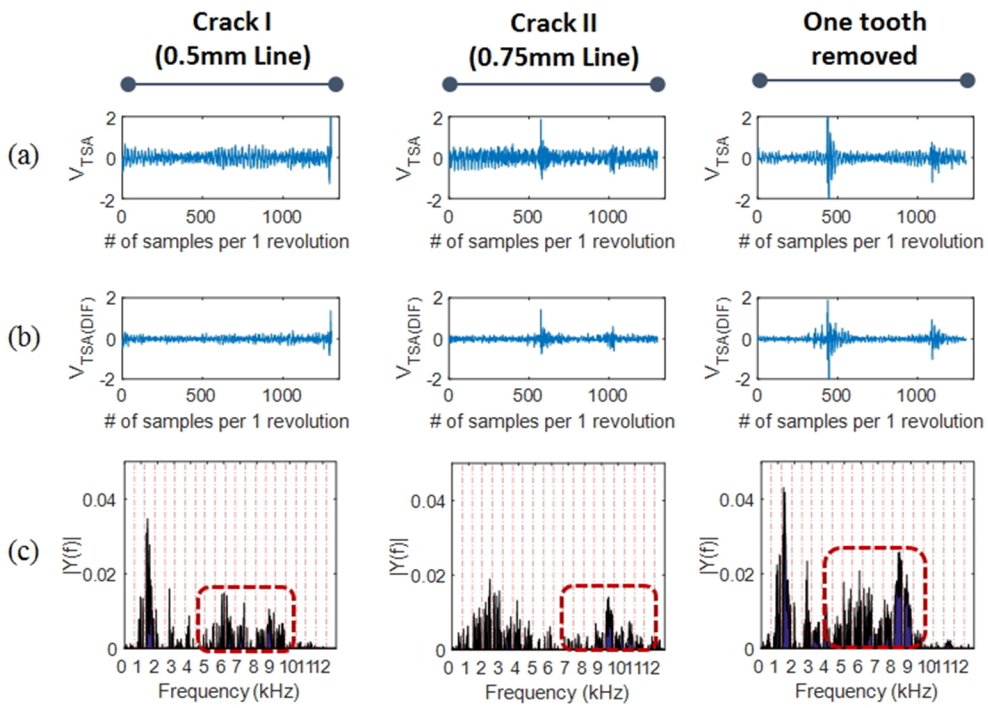

Figure 4-5 Reference sensor results from the use of TSA in a WT RIG tester

(a): TSA signal, (b) Difference signal, (c) FFT residual signal

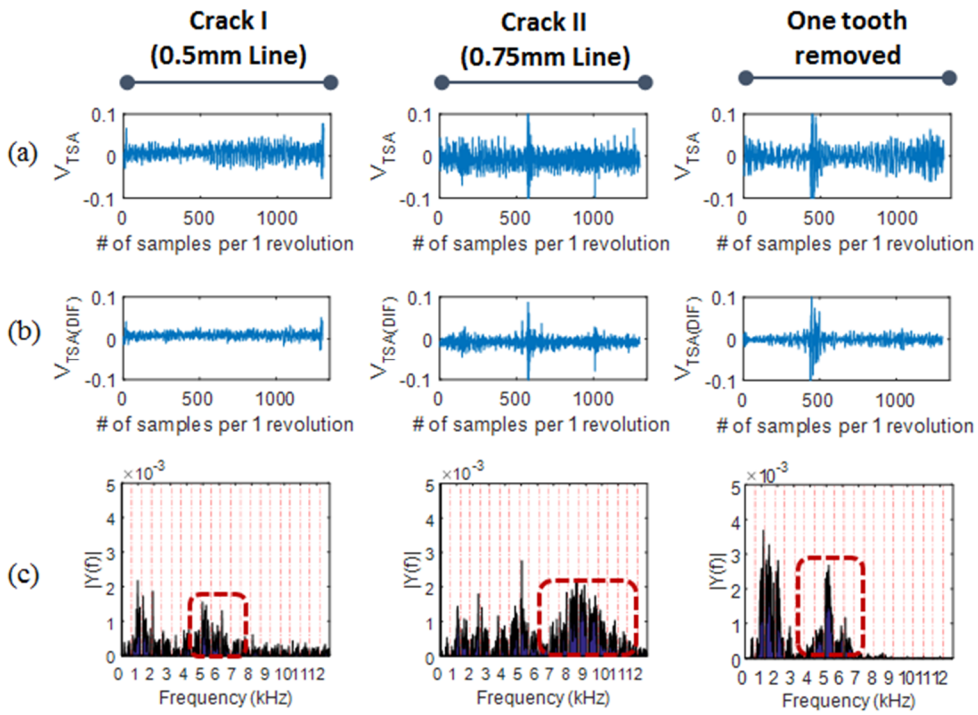

Figure 4-6 Knock sensor results from the use of TSA in a WT RIG tester

(a): TSA signal, (b) Difference signal, (c) FFT residual signal

(b) AR-MED

The use of an AR-MED filter results in the identification of peaks that arise due to faults in the time domain and the fault frequency domain; these peaks appear in the frequency domain. In the 4-line graph, the upper two lines represent the time and frequency domain signals of the raw signal and the lower two lines represent the time and frequency signals of the AR-MED filtered signal. When examining the results of these graphs, it is important to compare the signal shape, rather than the scale difference in the y-axis, because the sensitivity of each sensor is different.

Figures 4-7 and Figure 4-8 show the AR-MED results of the reference sensor and the knock sensor, respectively, considering the size of the fault in the WT RIG tester. For both sensors, as the size of the fault increases, the emphasis on the impact of the fault due to filtering also increases. It can be confirmed that only the frequency domain that is due to the fault is left after FFT of the filtered signal (AR residual signal). In the WT RIG tester, it is confirmed that the resulting signal is centered on about 10 kHz. However, in the results from both sensors for Crack I with a size of 0.5 mm, the results contained many other frequency components. In the case of the reference sensor, the peaks appeared to be well emphasized in the filtered signal in the time domain. No apparent fault frequency pattern was observed in the FFT results. In the knock sensor, emphasized peaks relative to the raw signal were not observed in the time domain. Therefore, when using the AR-MED filter, it is judged that the knock sensor in the WT RIG tester cannot detect a failure of 0.5 mm in size. In the case of the reference sensor, there is a possibility that detection of Crack I can be performed using an additional filter, such as a band-pass filter.

For the smallest fault in the excavator test, the peak of the filtered signal that

arises due to a fault in the time domain is not pronounced, and no definite fault frequency is observed in the frequency domain. In the case of the excavator, the vibration of the equipment itself and the vibrations of the surrounding components of the target gearbox may cause the detection performance to be lower than what is observed for the RIG tester performed in the laboratory. In addition, while the smallest crack size studied is the same as in the RIG, in the excavator the size of the gear is larger, so the detection difficulty is higher. In Crack IV, the fault frequency in the excavator's planetary gearbox is confirmed to occur at approximately 3 kHz center. In Crack V, an unusual phenomenon is confirmed. In the case of the reference sensor, the fault signal appears very well every time the faulty gear is meshed. If FFT is performed even before filtering, the frequency that is due to the fault, like the area indicated by the arrow, is clearly shown. There is a fault signal in all cases, so in the AR-MED filtered signal, the fault signal is recognized as a repetitive signal and thus can be seen to disappear.

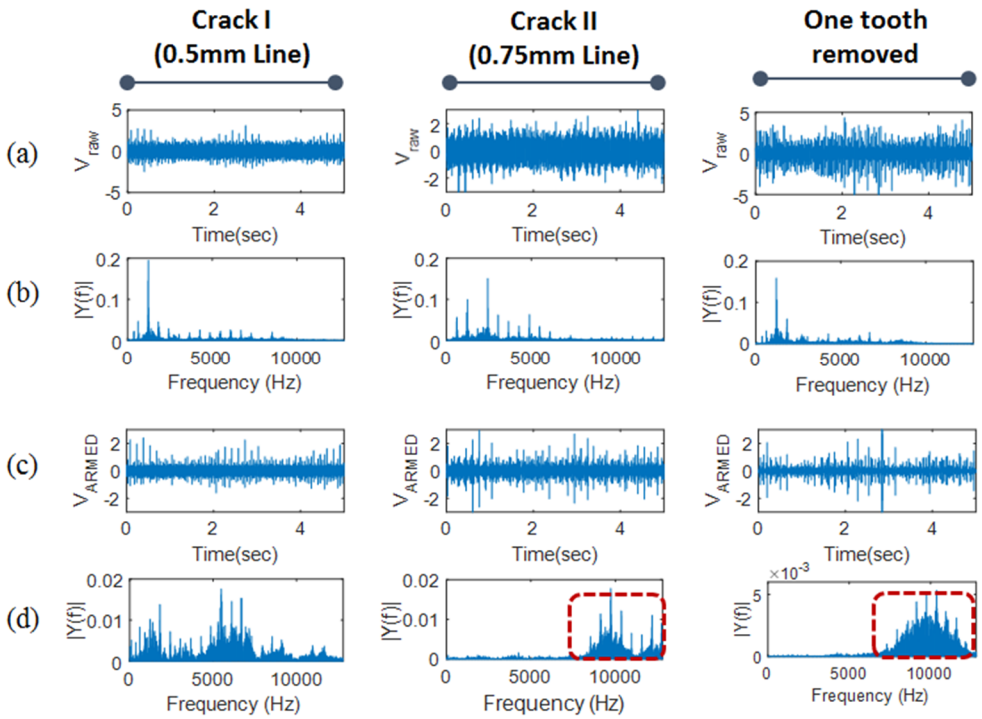

Figure 4-7 Reference sensor results from the use of AR-MED in the WT RIG tester

(a): Raw signal in the time domain, (b) FFT of the raw signal,

(c) Filtered signal in the time domain, (d) FFT of the filtered signal

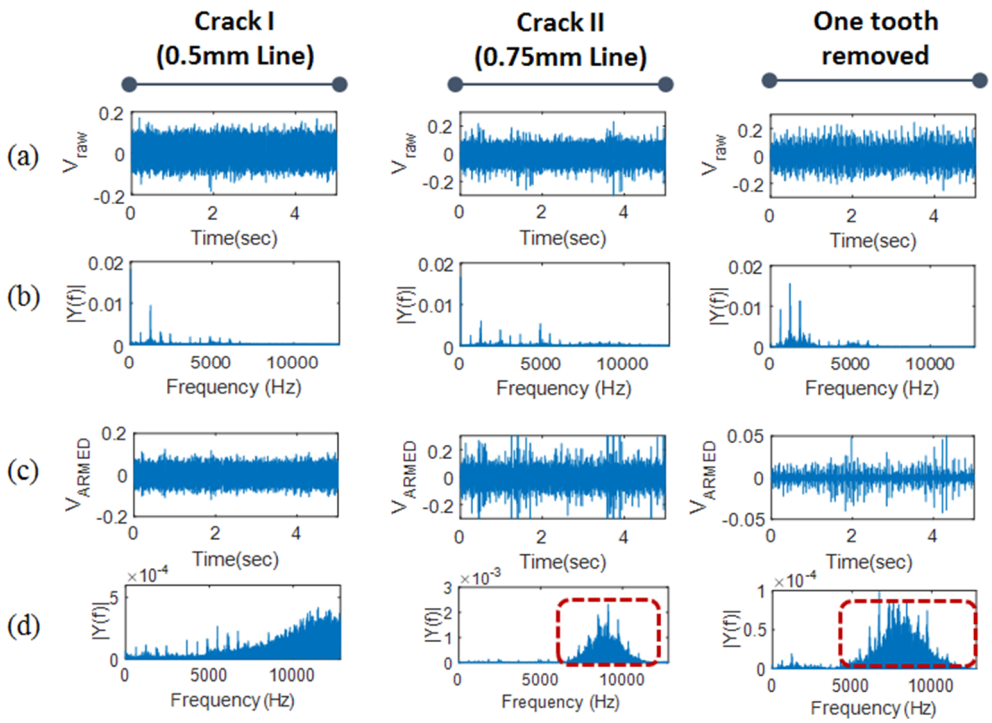

Figure 4-8 Knock sensor results from the use of AR-MED in the WT RIG tester

(a): Raw signal in the time domain, (b) FFT of the raw signal,

(c) Filtered signal in the time domain, (d) FFT of the filtered signal

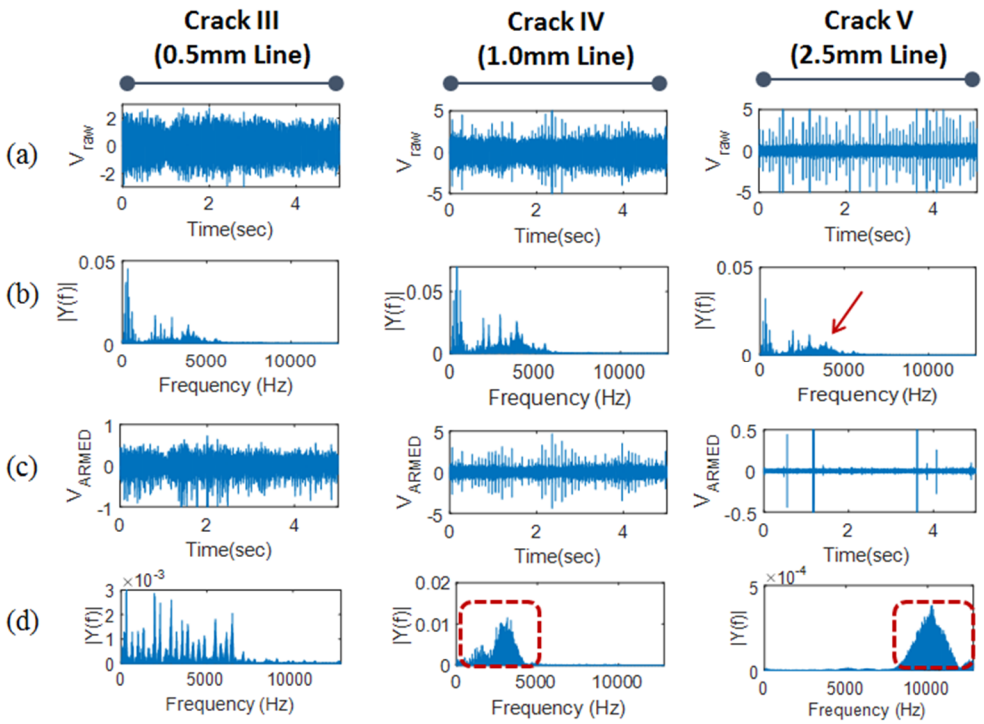

Figure 4-9 Reference sensor results from the use of AR-MED in the excavator

(a): Raw signal in the time domain, (b) FFT of the raw signal,

(c) Filtered signal in the time domain, (d) FFT of the filtered signal

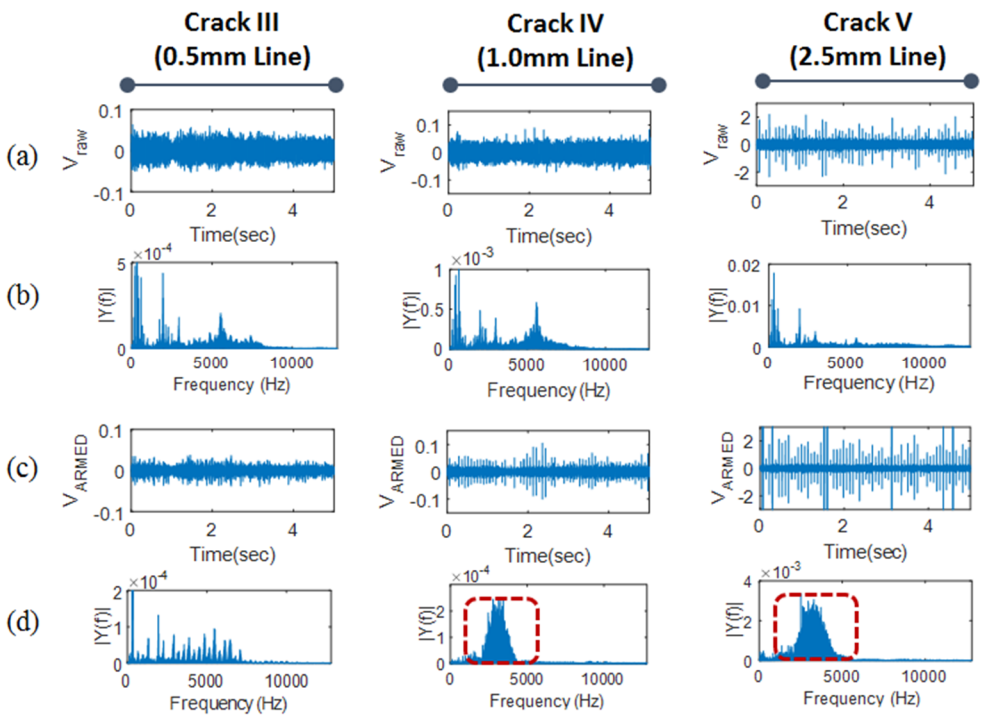

Figure 4-10 Knock sensor results from the use of AR-MED in the excavator

(a): Raw signal in the time domain, (b) FFT of the raw signal,

(c) Filtered signal in the time domain, (d) FFT of the filtered signal

c) SK

SK can identify the frequency region that arises from a failure more clearly than the two previously described methods. In the FFT of the AR-MED filtered signal, the frequency domain due to a failure can be identified in a certain frequency range. However, SK can define this more precisely, because it finds a region with high kurtosis while gradually dividing the frequency. By finding the highest kurtosis through band-pass filtering and envelope analysis of the signals, it is possible to check whether the frequency caused by the fault periodically appears. The magnitude of the frequencies representing the periodicity of the fault, including the fault's harmonics in the envelope analysis results, will affect the judgment of the fault in the quantitative comparison provided in the next chapter.

Figure 4-11 shows the results of applying SK to the raw signal provided from the reference sensor in the WT RIG tester. Considering the input speed and gear ratio of the system briefly described above, there are two cases in which the repetition period of frequency due to failure are as follows: 1) Crack I & Crack II - 19.7Hz when a faulty planetary gear meshes with the normal sun gear, or vice-versa and 2) One tooth removed - 39.3Hz when the fault of the planetary gear meshes with the sun gear and the ring gear, respectively. Figure 4-11 (a) shows the band-pass filtered signal with frequency information (i.e., center frequency and bandwidth) of the frequency range with the highest kurtosis. Peaks due to the fault are noticeable even for the smallest crack, Crack I. In addition, the frequency indicating the periodicity of the fault signal obtained through envelope analysis is also very clear. In the knock sensor results in Figure 4-12, it is judged that the fault is detected well by the filtering, except that the frequency indicating the fault periodicity is weak for the results of Crack I. The results of both sensors using SK

showed a filtered frequency range of 7 kHz to 11 kHz, which is similar to the frequency range that arises due to fault that is identified by the AR-MED filter.

In Figure 4-13 and Figure 4-14, which show the results of the excavator case, the fault frequency of 13Hz was confirmed by envelope analysis for Crack III (the smallest, 0.5mm crack) in both sensors; however, various other frequency components appeared dominant. The fault frequency was limited to a narrow band width in the frequency range lower than the WT RIG tester. It is presumed that various factors, such as system factors and driving conditions are combined.

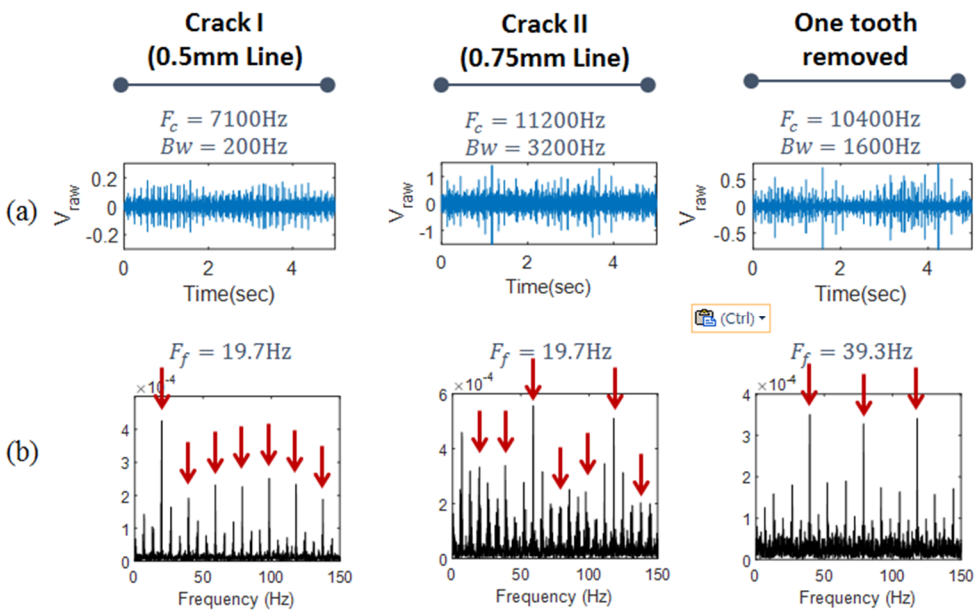

Figure 4-11 Reference sensor results from the use of SK in the WT RIG tester

(a): Band-pass filtered signal in the time domain, (b) FFT of the enveloped signal

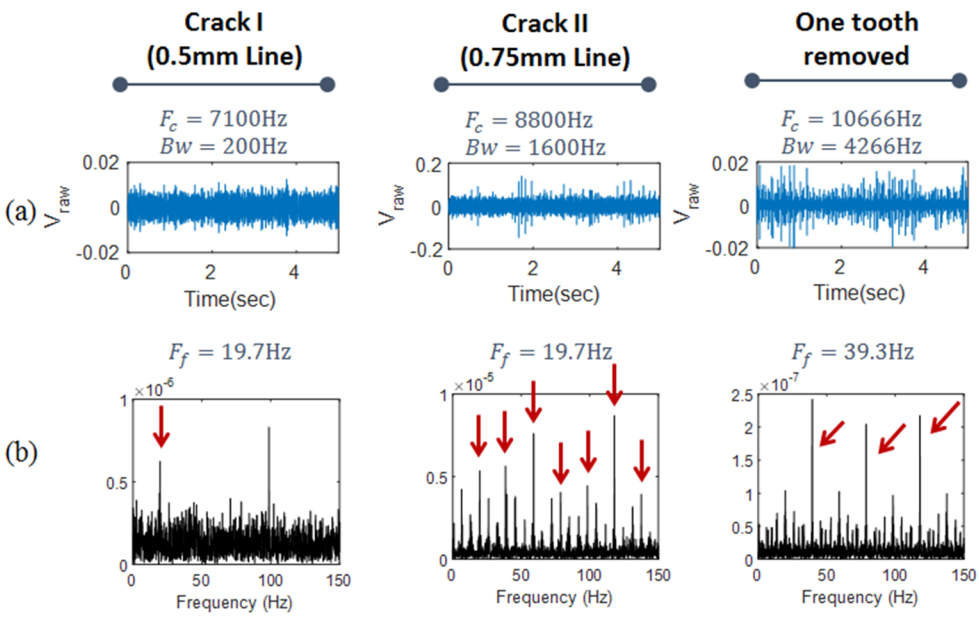

Figure 4-12 Knock sensor results from the use of SK in the WT RIG tester

(a): Band-pass filtered signal in the time domain, (b) FFT of the enveloped signal

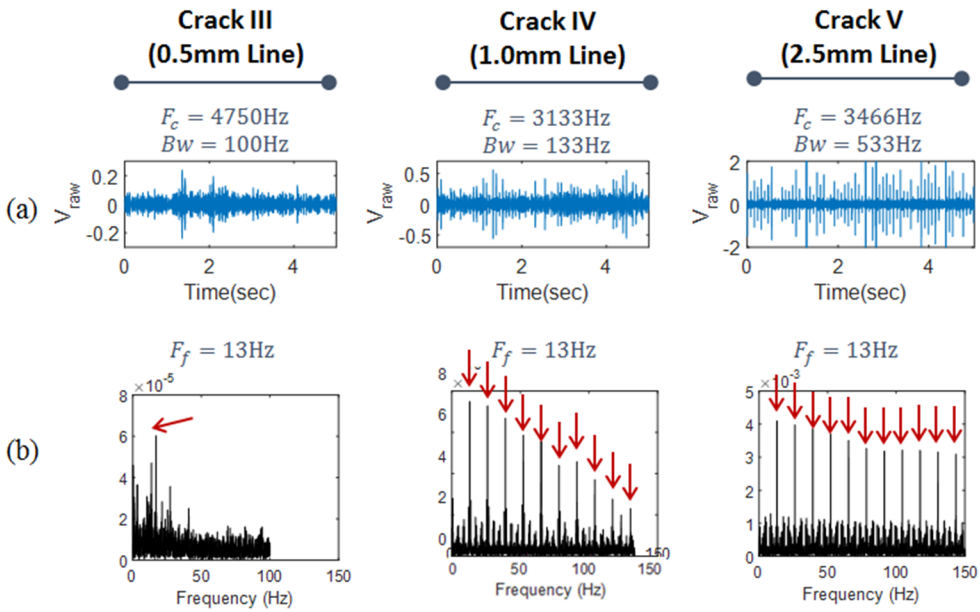

Figure 4-13 Reference sensor results from the use of SK in the excavator

(a): Band-pass filtered signal in the time domain, (b) FFT of the enveloped signal

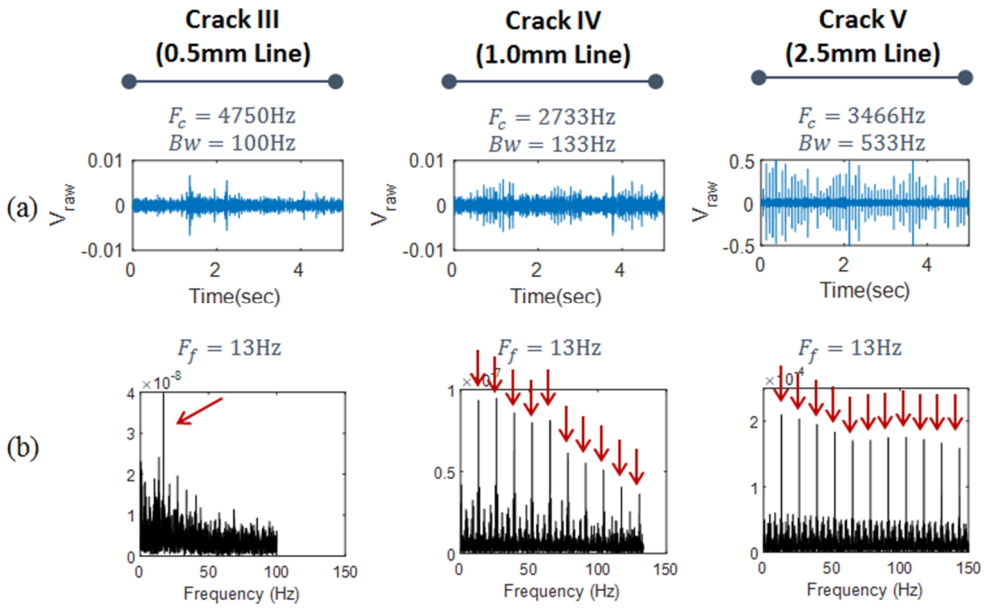

Figure 4-14 Knock sensor results from the use of SK in the excavator

(a): Band-pass filtered signal in the time domain, (b) FFT of the enveloped signal

d) Comprehensive Comparison of Results

Sections a) to c) of Chapter 4.3.2 compare five results with three signal processing methods that are applied to the three faulty specimens in the two systems. A comprehensive comparative analysis of these results is presented in Table 4-5. TSA, which is primarily aimed at noise reduction, has clearly distinguished all fault signals in the time domain. However, since there are various frequency components, including the GMF, in the frequency domain, it is difficult to distinguish the frequency range related to the fault. Because ARMED utilizes AR filters to remove regular signals, signals related to faults (i.e., irregular peaks) are clearly visible after filtering. However, if the vibration caused by the fault is small, the AR filters may not function properly. It is difficult to distinguish the smallest fault studied in both target systems. Conversely, in almost all of the fault gear meshing conditions studied, when a peak due to a fault is detected – such as the reference sensor for Crack V – the detection performance is deteriorated because all of the peaks that arise due to the fault are treated as repetitive signals. SK detected a similar fault frequency range for each system, independent of the size of the fault. This result reflects well the conclusions of the research that the frequency component of the impact-type fault occurs in the natural frequency range of the system.

Table 4-5 Comprehensive comparison of fault frequency identification by three signal processing methods

Signal Process	Target System	Fault Case	Sensor*	Fault Frequency Identification		
				Detectability		Frequency Range [kHz]
				Time Domain	Frequency Domain	
TSA	WT RIG	Crack I (0.5mm)	R	O	△	5 to 10
			K	O	△	4 to 12
		Crack II (0.75mm)	R	O	△	9 to 11
			K	O	△	
		One tooth removed	R	O	△	5 to 10
			K	O	△	4 to 7
ARMED	WT RIG	Crack I (0.5mm)	R	O	△	4 to 6
			K	X	X	X
		Crack II (0.75mm)	R	O	O	9 to 11
			K	O	O	
		One tooth removed	R	O	O	8 to 12
			K	O	O	6 to 12
	Excavator	Crack III (0.5mm)	R	△	X	X
			K	△	X	X
		Crack IV (1.0mm)	R	O	O	3 to 5
			K	O	O	
		Crack V (2.5mm)	R	O	△	3 to 5
			K	O	O	
SK	WT RIG	Crack I (0.5mm)	R	-	O	7.1 ± 0.1
			K	-	△	
		Crack II (0.75mm)	R	-	O	11.1 ± 1.6
			K	-	O	8.8 ± 0.8
		One tooth removed	R	-	O	10.5 ± 0.8
			K	-	O	10.5 ± 2.1
	Excavator	Crack III (0.5mm)	R	-	△	4.7 ± 0.1
			K	-	△	
		Crack IV (1.0mm)	R	-	O	3.1 ± 0.1
			K	-	O	2.7 ± 0.1
		Crack V (2.5mm)	R	-	O	3.5 ± 0.3
			K	-	O	

* R = Reference sensor, K = Knock sensor

4.3.3 Comparison of Diagnostic Performance using Quantitative Metrics

As confirmed in previous chapters, it has been found that the results of filtering using signal processing methods for the encoderless condition show a signal that is left with only the signals that arise due to a fault. The process of calculating the quantitative metric using these signals is as follows.

Step 1: Cut normal and faulty signals to the HTC length of each system
Step 2: Filter the clipped signals using each signal processing method
Step 3: Calculate health data (i.e., M8A) based on the filtered signal
Step 4: Calculate class separation metrics (i.e., PoS and FDR) using the distribution of M8A values

A comparison of the results of fault diagnosis performance for the two sensors is then compared with FDR when the normal and fault cases are completely separated. Detailed information can be obtained through the PoS when the normal and fault cases are partially separated. In each figure, fault cases are denoted by (a), (b), and (c), which correspond to Crack I, Crack II, and "One tooth removed" in the WT RIG results. Excavator results indicate Crack III, Crack IV, and Crack V, respectively.

a) Results for the WT RIG Tester

In Figure 4-10 (b) and (c), the value of PoS is 1. This indicates that the distributions of normal and faulty features can be completely separated to provide 100% fault detection. For the smallest fault (a), the reference sensor showed a failure detection rate of at least 69%, but the knock sensor showed only 40% fault

detection when using TSA. The results of AR-MED and SK filtering show that some fault frequencies were found through the use of the knock sensor; however, the vibration from the fault was too small compared to other vibration components and it was thus impossible to detect the fault.

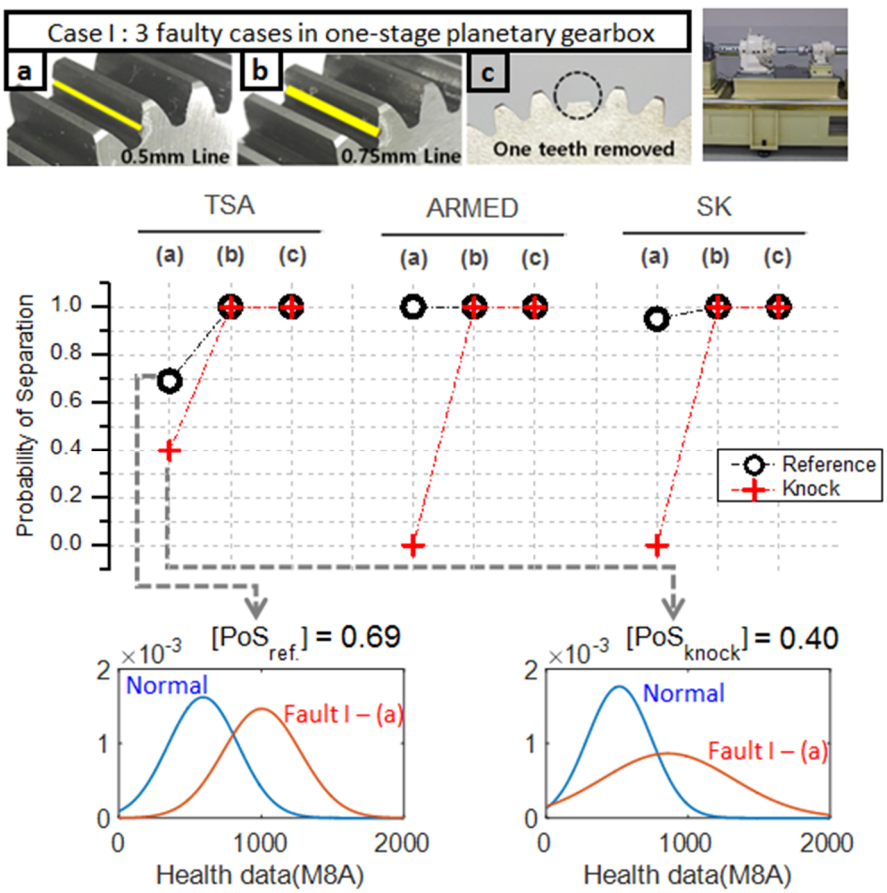

Figure 4-15 PoS results for the WT RIG tester

Figure 4-16 shows the FDR results. Even if the probability of fault detection (i.e., PoS) is similar, comparing the values of FDR can confirm the margin for

detectability of the different fault sizes. The larger the margin, the higher the resolution for fault detection based on fault size in each methodology. This can be a very significant value. In the case of TSA (b), that is, from the 0.75 mm line and larger, it can be seen that the signal resulting from the size of the fault is more dominant in the fault detection than the filtering effect that is due to the noise reduction. As a result of the other two signal processing methods, the separability increases as the size of the fault increases. Thus, it can be understood that those methods are highly dependent on the size of the fault. In (b), the results of AR-MED, the difference in FDR value between the two sensors is large because the impact signals due to the fault are more prominent in the reference sensor, as shown in the time domain signal in Figure 4-6.

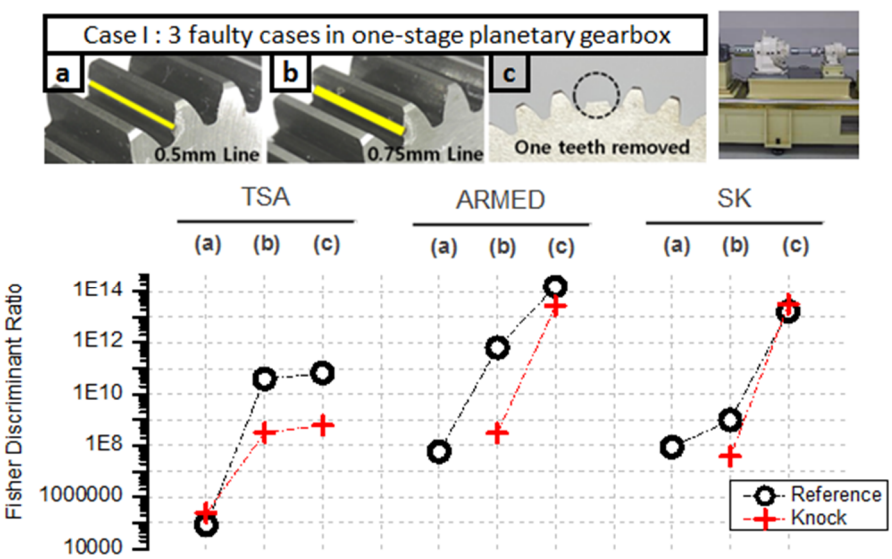

Figure 4-16 FDR results for the WT RIG tester

b) Results for the Excavator

The PoS results for the excavator are shown in Figure 4-17. In this case, TSA is not applied because the tach-signal cannot be used. In the case where AR-MED is applied to the smallest fault size, the fault and normal conditions were partially separated. The reference sensor showed 77% separability; the knock sensor showed only 54% separability.

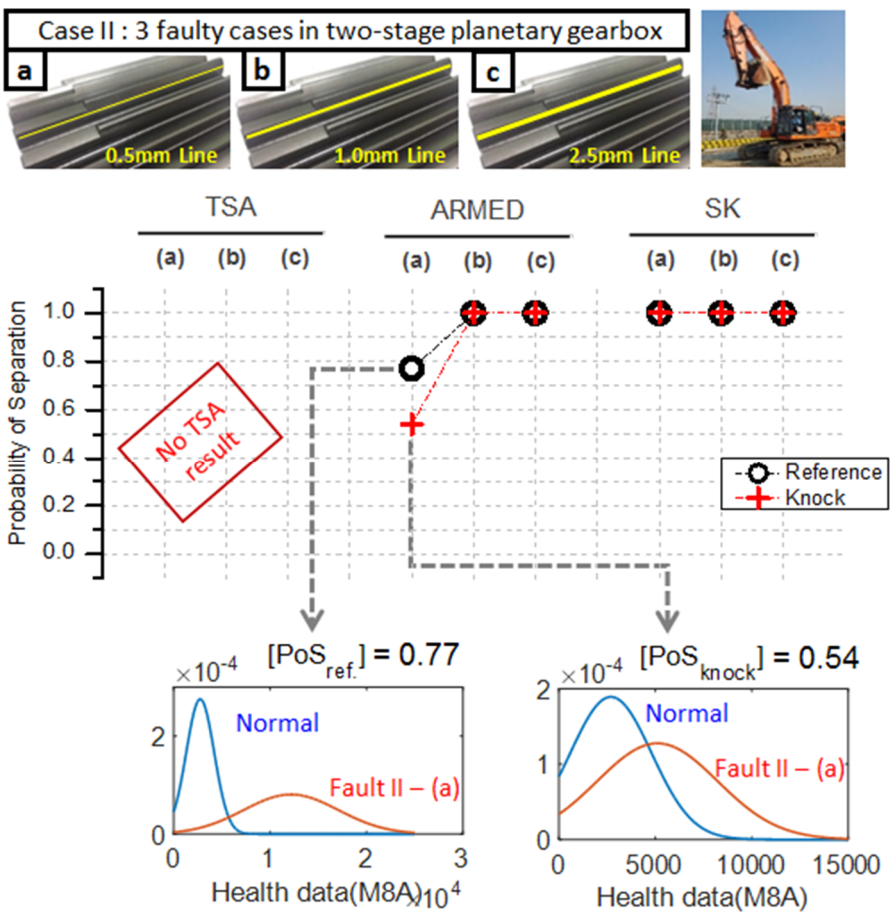

Figure 4-17 PoS result for the Excavator

The results of FDR showed that there are similar tendencies between the two signal processing methods, as shown in Figure 4-18. Through PoS and FDR, the reference sensor can correctly determine a 0.5mm line crack and the knock sensor can identify a 1.0mm line crack as the minimum fault detection limit for fault diagnosis of the excavator. Although the margin of fault detection is smaller than that of the reference sensor, if an SK filter is used at a specific fault level or higher, a fault detection performance similar to that of the reference sensor can be obtained.

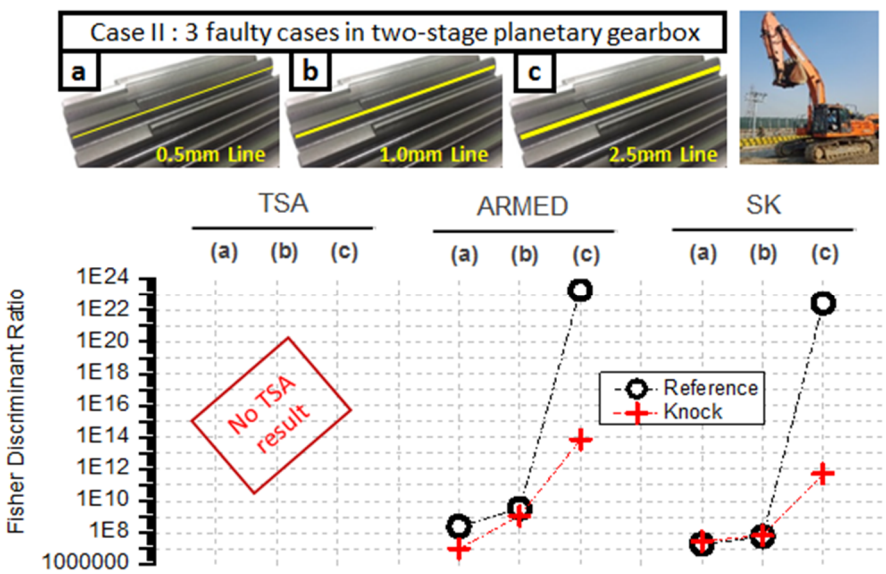

Figure 4-18 FDR result for the Excavator

Chapter 5. Conclusions and Future Work

5.1 Conclusions and Contributions

This thesis proposes a method for quantitatively evaluating the applicability of a low-cost accelerometer for fault diagnosis of a planetary gearbox in an excavator.

Research thrust 1 evaluates the vibration measurement performance of a knock sensor selected as a low-cost accelerometer for fault diagnosis. A commonly used accelerometer is used as a reference sensor, and the frequency range for stable performance is selected by calculating an estimated value of the SNR. Next, the performance of fault diagnosis is evaluated for faulty gears with an impact type in which the frequency characteristics related to the fault are clearly displayed in the usable frequency range of the knock sensor.

TSA, which is widely used for fault detection in gears, is a reliable signal processing method that can reduce noise and provide fault-detection features that better reflect the characteristics of the fault. However, an encoder, which is an essential element of TSA, isn't installed in excavators. Therefore, signal processing methods that *do not* utilize time information must be used. However, these methods do not reflect the characteristics of the faults because they use only the kurtosis to achieve fault diagnosis. In order to overcome this problem, a new method is proposed to perform fault detection by estimating a TSA-based feature that reflects the nature of the fault. This method compares the signals that have been signal processed to provide reliable fault detection results.

Research thrust 2 addresses this problem by introducing a fault diagnosis method that estimates a TSA-based feature that reflects the characteristics of a fault. The proposed solution uses a signal processing method that does not use time information. The signal-processed signals are compared to verify that this methodology provides reliable fault-detection.

The test for evaluating fault diagnosis performance was conducted with three failure specimens in both a RIG test and a vehicle test. Vibration data from both sensors were used to calculate features for fault diagnosis through three signal processing methods. Detectability of the faults was shown through the class separation metrics that utilized the distribution of this feature. The results show that the knock sensor has about 30% less fault detectability than the reference sensor for very small faults; however, the knock sensor has fault detection performance that is similar to the reference sensor for faults over a certain level.

5.2 Future Work

1) More fault types and levels should be considered

   Faulty specimens were selected from past research and were referred to in previous studies. In order to put this research into practical use, it will be necessary to select minimum fault detection criteria for each sensor and each signal processing method through additional experiments that examine the type and level of additional faults.

2) Surroundings should be considered

- Extended application of the fault diagnosis methodology

The frequency component of the other gears that constitute the two-stage planetary gearbox, which is the target of the proposed fault diagnosis, should be evaluated to consider the possibility of extending the methodology constructed through this study.

- Diagnose various parts using the vibration signal of the sensor

The second stage sun gear of the swing reduction gear of the excavator was selected as the fault diagnosis target through FMECA. However, analysis of the frequency spectrum confirmed various rotational frequencies. Based on this, it will be necessary in future work to study the possibility of detecting the fault frequency of the input shaft of the planetary gear box or the output shaft's related rotors.

- Reinforcing robustness of the methodology for various operating conditions

A precondition of the present study is that vibration data must be obtained in a constant torque and speed condition. Algorithms must be modified and supplemented to ensure performance even under varying operating conditions. For this reason, it will be necessary to reconstruct the angular information under the encoderless condition or to conduct additional research through time-frequency analysis.

Bibliography

1. Arakawa, S. (2002). Development and Deployment of KOMTRAX STEP 2. *Komatsu technical report,* 48(150), pp. 8-14.

2. He, Q. H., He, X. Y., & Zhu, J. X. (2008). Fault detection of excavator's hydraulic system based on dynamic principal component analysis. *Journal of Central South University of Technology*, 15(5), 700.

3. Zakrajsek, J. J., Townsend, D. P., & Decker, H. J., (1993). An analysis of Gear Fault Detection Methods as Applied to Pitting Fatigue Failure Data, *The Systems Engineering Approach to Mechanical Failure Prevention*, 47th Meeting of MFPG.

4. R. M. Stewart, "Some Useful Data Analysis Techniques for Gearbox Diagnostics," 1977.

5. Martin, H.R., (1989). *S*tatistical Moment Analysis As a Means of Surface Damage Detection, *Proceedings of the 7th International Modal Analysis Conference, Society fur Experimental Mechanic*s, Schenectady, MY, pp. 1016-1021.

6. Li, Y., Ding, K., He, G., & Lin, H. (2016). *Vibration mechanisms of spur gear pair in healthy and fault states*. Mechanical Systems and Signal Processing, 81, pp. 183-201

7. McFadden, P. D. (1987). Examination of a technique for the early detection of failure in gears by signal processing of the time domain average of the meshing vibration. *Mechanical Systems and Signal Processing*, vol. 1 (2), pp. 173–183.

8. Endo, H., & Randall, R. B. (2007). Enhancement of autoregressive model based gear tooth fault detection technique by the use of minimum entropy deconvolution filter. *Mechanical Systems and Signal Processing*, 21(2), pp. 906-919.

9. Antoni, J., & Randall, R. B. (2006). The spectral kurtosis: application to the vibratory surveillance and diagnostics of rotating machines. *Mechanical Systems and Signal Processing*, 20(2), pp. 308-331.

10. LEBOLD, Mitchell, et al. Review of vibration analysis methods for gearbox diagnostics and prognostics. In: *Proceedings of the 54th meeting of the society for machinery failure prevention technology*. 2000. p. 16.

11. JEON, Byung Chul, et al. Datum unit optimization for robustness of a journal bearing diagnosis system. *International Journal of Precision Engineering and Manufacturing*, 2015, 16.11: 2411-2425.

12. S. Theodoridis and K. koutroumbas, *Pattern Recognotion*: Elsevier Science, 2008.

13. CERTIFICATION, GL Renewables. Guideline for the Certification of Condition Monitoring Systems for Wind turbines. *Hamburg: GL Renewables Certification*, 2013.

14. SHIEH, J., et al. The selection of sensors. *Progress in materials science*, 2001, 46.3: 461-504.

15. ALBARBAR, A., et al. Performance evaluation of MEMS accelerometers. *Measurement*, 2009, 42.5: 790-795.

16. ALBARBAR, Alhussein, et al. Suitability of MEMS accelerometers for condition monitoring: An experimental study. *Sensors*, 2008, 8.2: 784-799.

17. PIPITONE, Emiliano; D'ACQUISTO, Leonardo. First experience with a piezo film based knock sensor. In: *2nd International Workshop on Modeling, Emissions and Control of Automotive Engines, Salerno, Italy*. 2002.

18. JOHNSON, Don H. Signal-to-noise ratio. *Scholarpedia*, 2006, 1.12: 2088.

19. ORFANIDIS, Sophocles J. *Introduction to signal processing*. Prentice-Hall, Inc., 1995.

20. STANDARD, I. International Standard ISO 16063-21. Methods for the calibration of vibration and shock transducers. 2003.

21. AMBARDAR, Ashok. *Analog and digital signal processing*. PWS Publishing Company, 1995.

22. JONES, Derek K. *Diffusion mri*. Oxford University Press, 2010.

23. GAVRILOVSKA, Liljana; PRASAD, Ramjee. *Ad hoc networking towards seamless communications*. Heidelberg: Springer, 2006.

24. LENT, B. Practical considerations of accelerometer noise. *Endevco Website< https://www. endevco. com/news/arc hivednews/2009/2009_12/TP324. pdf>(Dec. 18. 2015)*, 2007.

25. LEI, Yaguo, et al. Condition monitoring and fault diagnosis of planetary gearboxes: A review. *Measurement*, 2014, 48: 292-305.

26. Chaari, T. Fakhfakh, M. Haddar, Analytical investigation on the effect of gear teeth faults on the dynamic response of a planetary gear set, *Noise & Vibration Worldwide* 37 (2009) 9–15.

27. Z.W. Wang, Dynamic modelling of planetary gear systems for gear tooth fault detection, Master Thesis, Curtin University of Technology, Perth, Australia, 2010.

28. Z. Cheng, N.Q. Hu, Quantitative damage detection for planetary gear sets based on physical models, *Chinese Journal of Mechanical Engineering* 24 (2011) 1–7.

29. C.M. Vicuña, Theoretical frequency analysis of vibrations from planetary gearboxes, *Forsch Ingenieurwes* 76 (2012) 15–31.

30. S. Jain, H. Hunt, Vibration response of a wind-turbine planetary gear set in the presence of a localized planet bearing defect, in: *ASME 2011 International Mechanical Engineering Congress and Exposition (IMECE2011)*, Denver, Colorado, USA, November 11–17, 2011, pp. 943–952.

31. P.D. McFadden, A technique for calculation the time domain averages of the vibration of the individual planet gears and the sun gear in an epicyclic gearbox, J*ournal of Sound and Vibration* 144 (l) (1991) 163–172.

32. P.D. McFadden, I.M. Howard, The detection of seeded faults in an epicyclic gearbox by signal averaging of the vibration, *Technical Report, Propulsion Report* 183, Aeronautical Research Laboratory, Melbourne, Australia, October 1990.

33. B.Q. Wu, A. Saxena, T.S. Khawaja, et al., An approach to fault diagnosis of helicopter planetary gears, in: *Autotestcon 2004 Proceedings*, Atlanta, GA, USA, September 20–23, 2004, pp. 475–481.

34. B.Q. Wu, A. Saxena, R. Patrick, et al., Vibration monitoring for fault diagnosis of helicopter planetary gears, in: *Proceedings of the 16th IFAC World Congress*, Prague, 2005, pp. 126–131.

35. J.A. Keller, P. Grabill, Vibration monitoring of UH-60A main transmission planetary carrier fault, in: American Helicopter Society 59th Annual Forum, Phoenix, Arizona, USA, May 6–8, 2003.

36. J. McNames, Fourier series analysis of epicyclic gearbox vibration, *Journal of Vibration and Acoustics* 124 (2001) 150–152

37. CHAARI, Fakher, et al. Gearbox vibration signal amplitude and frequency modulation. *Shock and Vibration*, 2012, 19.4: 635-652.

38. VILLA, Luisa F., et al. Statistical fault diagnosis based on vibration analysis for gear test-bench under non-stationary conditions of speed and load. *Mechanical Systems and Signal Processing*, 2012, 29: 436-446.

39. D. G. Lewicki, R. T. Ehinger, and J. Fetty, "Planetary Gearbox Fault Detection Using Vibration Separation Techniques," 2011.

국문 초록

기어 박스는 회전체의 핵심 부품 중 하나로써, 기어 박스 결함에 대한 시기 적절한 예측은 갑작스럽게 발생하는 고장에 의한 장비 정지 시간을 최소화하는 데 매우 중요하다. 대부분의 기어박스 고장 진단 연구는 값비싼 진동 센서를 사용하는 진단 알고리즘의 개발에 중점을 두고 있다. 그러나 고장 진단 대상 시스템에 따라 진동 센서의 비용에 대한 중요도가 다르므로, 일부 어플리케이션에서는 저가의 센서 적용이 요구된다. 이 연구에서는 디젤 엔진과 같이 고주파수의 충격 진동을 감지해야 하는 경우에 비용 효율성과 성능이 좋은 것으로 알려진 노크 센서가 장착된 유성 기어 박스를 사용한다.

이 연구는 고장 진단을 위한 정량적 센서 평가 프로세스를 개발하는 데 그 목적이 있다. 센서의 성능은 진동 측정 및 고장 진단 측면에서 비교 대상인 기준 센서와 비교 평가된다. 진동 측정 성능은 신호 대 잡음 비 (SNR)를 추정한 값을 통해 평가되고, 고장 진단 성능은 기어 박스의 건전성 데이터 엔지니어링을 통해 정상 상태와 결함이 있는 기어에서 각각 얻은 진동 신호를 분석하여 결함이 정상 상태와 분리되었는지 여부를 확인함으로써 평가된다.

이 연구에서는 두 가지 아이디어가 제안 될 것이다. 첫째, 센서의 성능을 평가하는 데 있어서 몇 가지 정량적 측정 기준을 사용할 것이다. 노크 센서의 진동 성능은 신호 대 잡음 비 (SNR)를 추정하여 평가에 활용한다. 고장 진단을 위한 노크 센서의 안정된 주파수 범위는 SNR 값을 기반으로 정의될 것이다. 고장 진단 평가의 관점에서 고장 분리 능력은 분리 확률 (PoS) 및 피셔 판별 비율 (FDR)에 의해 성능이 평가될 것이다. 둘째, 고장 진단을 위해 사용된 건전성 데이터의 기본

신호에 대한 새로운 적용 방안이 제안될 것이다. 기어의 고장 진단에는 일반적으로 신호의 노이즈를 줄이는 목적의 시간 동기 평균화 (TSA) 방법을 통해 고장의 특성을 반영하는 건전성 데이터를 추출하는 방법이 사용된다. TSA는 엔코더 신호를 활용한 회전체의 각도 정보가 필수적이고, 그렇지 않은 경우에 사용할 수 있는 신호 처리 방법들 (자기 회귀 – 최소 엔트로피 역회선 (AR-MED) 및 스펙트럼 첨도 (SK))은 고장의 특성에 대한 고려 없이 첨도를 건전성 데이터로 활용한다. 이러한 신호 처리 방법들에 TSA 기반의 건전성 데이터를 계산하는 방법을 적용하면, 엔코더가 없는 상태에서도 고장의 특성이 고려된 건전성 데이터를 구할 수 있다. 새롭게 구해진 건전성 데이터는 신호 처리 결과에서 고장 신호의 주파수 범위와 주기성을 분석하여 유의미함을 검증하였다. 제안된 센서 평가 프로세스와 측정 기준의 효과를 입증하기 위해 풍력 터빈 리그 테스터와 굴삭기의 선회 감속 기어의 두 가지 사례 연구가 제시된다.

저가형 센서가 활용 가능한 주파수 영역에서 고장의 특성 주파수가 나타나는 고장 기어에 대하여 각도 정보를 사용하지 않는 신호 처리 방법을 통해 건전성 데이터를 구 해본 결과, 기어 박스의 고장 진단을 위해 노크 센서가 사용될 수 있다고 결론지었다.

주요어: 굴삭기 고장 진단
노크 센서
센서 성능 평가
정량적 메트릭

학 번: 2015-22705